การคำนวณทางควอนตัมของปฏิกิริยาอิพอกซิเดชันที่เร่งปฏิกิริยาด้วย

สารประกอบเชิงซ้อนแวนาเดียม

นายสิริชัย ลาวัณย์วิสุทธิ์

วิทยานิพนธ์นี้เป็นส่วนหนึ่งของการศึกษาตามหลักสูตรปริญญาวิทยาศาสตรมหาบัณฑิต
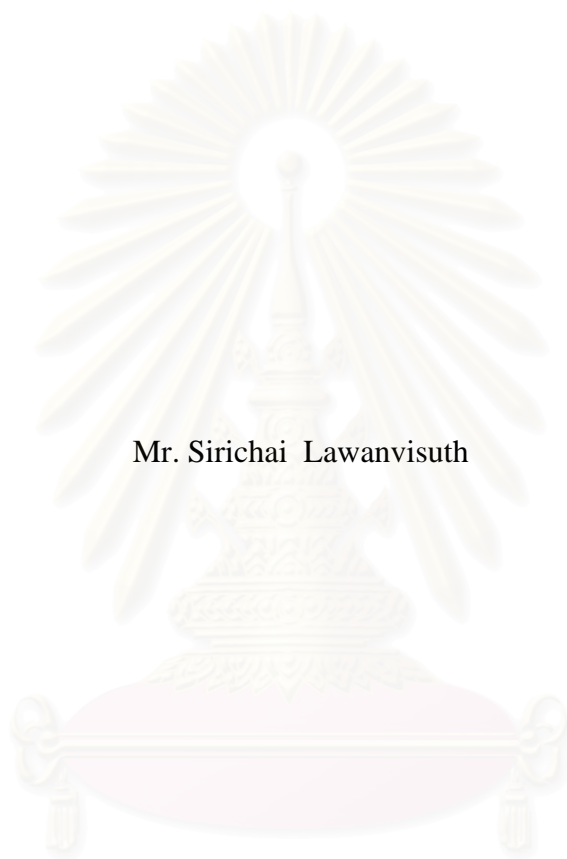
สาขาปิโตรเคมีและวิทยาศาสตร์พอลิเมอร์

คณะวิทยาศาสตร์ จุฬาลงกรณ์มหาวิทยาลัย

ปีการศึกษา 2547

ISBN 974-53-1615-6

QUANTUM CHEMICAL CALCULATION ON CATALYTIC EPOXIDATION BY
VANADIUM COMPLEX

Mr. Sirichai Lawanvisuth

Thhesis Title   Quantum Chemical Calculation on Catalytic Epoxidation by
                  Vanadium Peroxy Complex.

By   Mr.Sirichai Lawanvisuth

Field of Study   Petrochemistry and Polymer Science

Thesis Advisor   Associate Professor Vithaya Ruangpornvisuti, Dr. rer. nat.

Accepted by the Faculty of Science, Chulalongkorn University in Partial Fullfillment of the Requirements for the Master's Degree

.... Dean of the Faculty of Science.
(Professor Piamsak Menasveta, Ph. D.)

THESIS COMMITTEE

.... Chairman
(Professor Pattarapan Prasassarakich, Ph. D.)

.... Thesis Advisor
(Associate Professor Vithaya Ruangpornvisuti, Dr. rer. nat.)

.... Member
(Associate Professor Wimonrat Trakarnpruk, Ph. D.)

.... Member
(Associate Professor Thawatchai Tuntulani, Ph. D.)

สิริชัย ลาวัณย์วิสุทธิ์: การคำนวณทางเคมีควอนตัมของอิพอกซิเดชันที่เร่งปฏิกิริยาด้วยสารประกอบเชิงซ้อนแวนาเดียมเปอร์ออกซี (QUANTUM CHEMICAL CALCULATION ON CATALYTIC EPOXIDATION BY VANADIUM COMPLEX) อาจารย์ที่ปรึกษา รศ. ดร. วิทยา เรืองพรวิสุทธิ์, 57 หน้า. ISBN 974-1615-6

ได้ศึกษาปฏิกิริยาอิพอกซิเดชันของไครัลอะไลลิกแอลกอฮอล์ ได้แก่ 3-เมทิลบิท-3-อีน-2-ออล (r1), ทรานส์-เพนท์-3-อีน-2-ออล (r2) และ ซีส-เพนท์-3-อีน-2-ออล (r3) ด้วยระเบียบวิธีเดนซิตี้ฟังก์ชัน เบซิสเซท B3LYP/6-31G(d) สำหรับ ตัวออกซิแดนท์ $VO(OH)_3/H_2O_2$ โลหะแวนาเดียม(V) เกิดปฏิกิริยาแลกเปลี่ยนลิแกนด์กับไฮโดรเจนเปอร์ออกไซด์ และ อะไลลิกแอลกอฮอล์ ได้อย่างรวดเร็ว ดังขั้นที่ 1 และ 2 หลังจากนั้นเกิดปฏิกิริยาเคลื่อนย้ายออกซิเจนด้วยลักษณะอิเล็กโทรฟิรีกดังขั้นที่ 3 และขั้นสุดท้ายเกิดปฏิกิริยาแลกเปลี่ยนลิแกนด์ได้อิพอกไซด์และตัวเร่งปฏิกิริยากลับมา สำหรับแต่ละชนิดของสารตั้งต้น พลังงานอิสระของสารประกอบระหว่างปฏิกิริยา, สภาพทรานซิชันของ *threo* และ *erytho* และผลิตภัณฑ์ที่สอดคล้องกับปฏิกิริยาถูกนำมาคำนวณหาค่า อัตราส่วนผลิตภัณฑ์ *threo:erytho* หาค่าได้จากพลังงานอิสระของสภาพทรานซิชันของ *threo* และ *erytho* เท่ากับ 99.7:0.3, 80.9:19.1 และ 72.2:27.8 สำหรับ r1, r2 และ r3 ตามลำดับ

สาขา___ปิโตรเคมีและวิทยาศาสตร์พอลิเมอร์___ ลายมือชื่อนิสิต_____

ปีการศึกษา_____2547_____ ลายมือชื่ออาจารย์ที่ปรึกษา_____

.

4572534223: PETROCHEMISTRY AND POLYMER SCIENCE PROGRAM.

SIRICHAI LAWANVISUTH: QUANTUM CHEMICAL CACULATION ON
CATALYTIC EPOXIDATION BY VANADIUM COMPLEX.
THESIS ADVISOR: ASSOC. PROF. VITHAYA RUANGPORNVISUTI,
Dr. rer. nat., 57 pps. ISBN 974-53-1615-6

The epoxidation of three stereolabeled methyl-substituted chiral allylic alcohols with an allylic strain, namely 3-methylbut-3-en-2-ol (r1), trans-pent-3-en-2-ol (r2) and cis-pent-3-en-2-ol (r3), has been studied by the density functional theory method, B3LYP/6-31G(d). For the $VO(OH)_3/H_2O_2$ oxidant, the vanadium(V) metal rapidly exchanges its ligands for the hydrogen peroxide and allylic alcohol (step 1 and 2). The latter is coordinative activated for oxygen transfer through its enhanced electrophilic character (step 3). And final step is the ligand-substitution to give products and release catalysts. For each substrate, the free energies of intermediate complexes, their *threo* and *erytho* transition state, and the corresponding product complexes were calculated. The *threo*:*erytho* product ratios have been estimated from the computed free-energies for the competing *threo* and *erytho* transition states to be 99.7:0.3 (r1), 80.9:19.1 (r2) and 72.2:27.8 (r3).

Field of Study **Petrochemistry and Polymer Science** Student's signature

Academic year   2004   Advisor's signature

ACKNOWLEDMENTS

CONTENTS

LIST OF FIGURES

LIST OF TABLES

CHAPTER I

INTRODUCTION

The epoxidation of olefins is one of the most valuable reactions in organic synthesis and is even a subject of intensive study today. Particularly, catalytic and stereoselective epoxidations still present a major challenge. The epoxidation of alkenes is the most fundamental oxygen funtionalization of carbon-carbon double bonds.[1] The importance of this transformation is direct consequence of the utility of the product epoxides as synthetic intermediates. Accordingly, the ability to carry out enantioselective oxygen atom transfer to alkenes has served as the vanguard for advances in asymmetric catalysis such as the Sharpless epoxidation[2-6] of allylic alcohols and the Jacobsen epoxidation[7-10] of unfunctionalized olefins. In both cases, the stereoselectivity is controlled by optically active oxidizing species (reagent controls). Stereoselectivity may also be controlled by substituents at stereogenic center of chiral substrate (substrate control). The important requirements in the latter case are the conformation constraints on the chiral substrate and an efficient interaction (electronic, steric) with the reagent to facilitate preferential attack of the diastereotopic faces of the substrate.

1.1. Epoxidation of alkenes

Oxygen atom of epoxide is analogous to carbene (figure 1.1a). It has six electrons in its valance shell. It might be expected to act as both electrophile and nucleophile in its reaction with an alkene, resulting in the formation of three-membered ring epoxide (Figure 1.2b).

(a)   (b)

Figure 1.1. Structures of carbene (a) and epoxide (b).

An epoxide is three-membered cyclic ether, some time called an oxirane. Epoxides are valuable synthetic intermediates for organic chemistry, used to convert alkenes to a variety of other functional groups. Oxygen is added to carbon-carbon double bond to form epoxide. The oxidant, such as peroxyacids, dioxirane, peroxynitrous acid and oxaziridine can oxidize alkene to form epoxide but some reagents, peroxyformic acid, is strongly acidic. The epoxide opens to a glycol. Therefore, to make an epoxide, uses a weak acid such as peroxybenzoic acid. There are large amounts of data showing that the reaction rate is increased by electron donating group on the oxidant but that it is insensitive to the steric environment.

The mechanism of peroxy acid[11](Figure 1.2a) and peroxy nitrous[11] (Figure 1.2b) epoxidation is belived to include a cyclic-concerted transition state, in which oxygen is transferred to the alkene and the proton is transferred to carbonyl or nitronyl groups. And the mechanism of dioxirane[11-12](Figure 1.2c) and oxaziridine[13] (Figure 1.2d) epoxidation is predicted that oxygen is transferred to the alkene and the C-O or C-N is formed carbonyl or proton is transferred to carbonyl or nitryl groups.

(a)   (b)

(c)   (d)
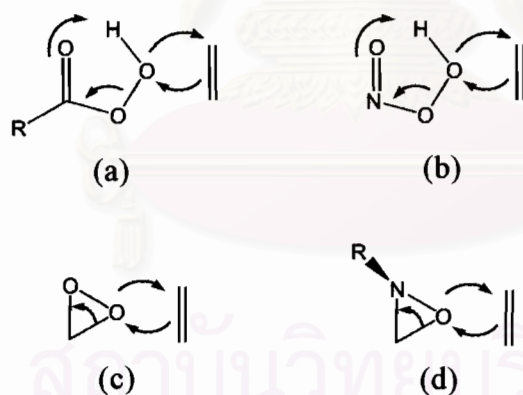
Figure 1.2. The cyclic-concerted transition state of epoxidation by peroxy acid (a), peroxy nitrous (b), dioxirane (c) and oxaziridine (d).

On the computational side, alkene epoxidations can be classified formally as to the nature of the substrate and type of oxidant into four main groups:[14] (i) symmetrical alkene (ethylene) and symmetrical oxidizing agents (peroxyformic acid and

peroxynitrous acid), which can form a spiro-type transition structure where the plane of the oxidant is at 90° to the double bond with equivalent bonds between the carbons and the spiro oxygen; (ii) symmetrical alkene and unsymmetrical oxidant (oxaziridine); (iii) unsymmetrical alkenes (propene) and symmetrical oxidant; (iv) unsymmetrical alkene and unsymmetrical oxidant. With the exception of the case i, where a strictly symmetrical approach is predicted on the basis of electronic considerations, an asymmetrical approach to the alkene double bond should occur. These generalizations do not preclude a variety of other possible transition structures if a planar approach of the oxidizing reagent to the C-C bond axis is preferred on steric grounds.

1.2 Epoxidation of alkene and alkyl peroxide catalyzed by transition-metal complexes

$$\text{(1.1)}$$
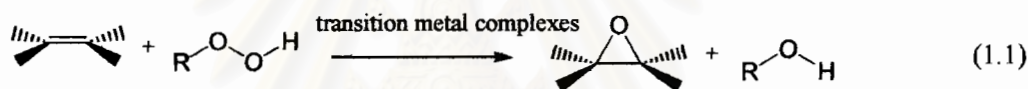
hydroperoxides Eq. 1.1 is a basic reaction to produce the epoxide using the transition metal complexes. The transition metal complexes are characterized as being Lewis acids in their highest oxidation state. These Lewis acids have a low redox potential and are labile with respect to ligand substitution. Transition-metal complexes in a high oxidation state, such as those of titanium(IV)[15-17], vanadium(V)[18], molybdenum (VI)[19], and tungsten(VI)[20], can facilitate the heterolysis of alkyl peroxides and of hydrogen peroxide by forming complexes analogous to the inorganic peracids formed with hydrogen peroxide. For synthesis, transition metal-alkyl hydroperoxide reagents are of more utility than the analogous transition metal-hydrogen peroxide reagents by virtue of their solubility in nonpolar solvents.[21-23]

The first step in the transition metal-catalyzed epoxidation with peroxides is the conversion of the peroxide to a peroxo-metal intermediate. For transition metal alkoxides this step leads to an exchange of one of the alkoxide ligands by the peroxide (Eq.1.2 or 1.3).

$$M(OR)_n + R'OOH \longrightarrow M(OR)_{n-1}(OOR') + ROH \qquad (1.2)$$

$$MO(OR)_n + R'OOH \longrightarrow M(OR)_n(OOR')OH \qquad (1.3)$$
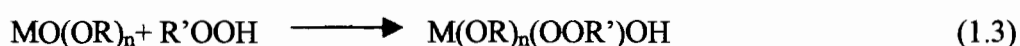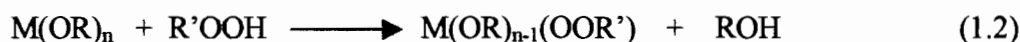
The exact structures of the transition-metal alkyl peroxide complex (products in Eq. 1.2 or 1.3) are unknown, but from vanadium- and molybdenum-catalyzed epoxidation[24-25] evidence has been provided through ^{18}O-labeling studies that the alkyl peroxide remains. The binding of the alkyl or hydrogen peroxide to transition metal in complex takes place via the terminal oxygen, but the other oxygen might be involved in the coordination to transition metal, leading to a bidentate coordinated transition metal complex. An *O-O* bound d^{o} peroxo complex such as shown in Figure 1.3a has recently been found in a (dipic)VO(OO-*t*-Bu)H$_2$O complex[24] (Figure 1.3b).

(a)   (b)
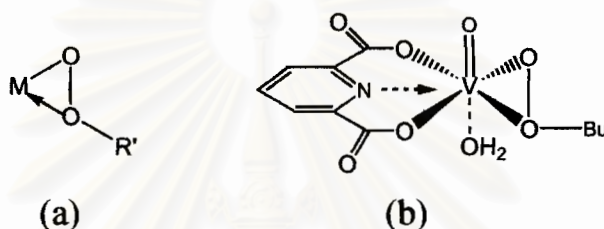
Figure 1.3. Coordination model of peroxo complex (a) and structure of (dipic)VO(OO-*t*-Bu)H$_2$O complex (b).

The coordination of the peroxide to transition metal as depicted, leads thus to an activation of the peroxide for oxygen transfer, and the following four mechanisms[26-28] have been suggested in Figure 1.4.
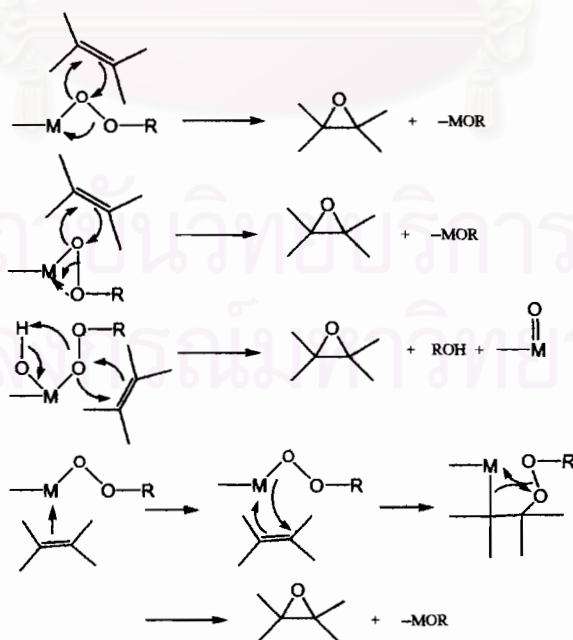
Figure 1.4. The mechanism of epoxidation by the transition metal complexes.

For epoxidation of allylic alcohols with vanadium-alkyl hydroperoxides, the mechanism shown in Figure 1.5 has been proposed.
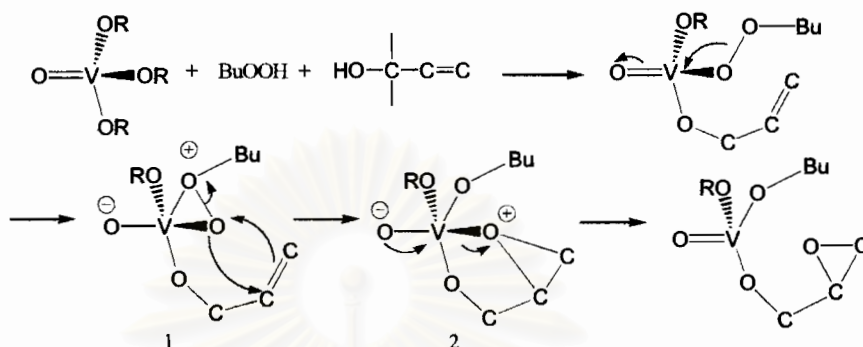
Figure 1.5. The pathway of epoxidation of allylic alcohols with vanadium-alkyl hydroperoxides.

The exceptional reactivity of the allylic alcohols toward vanadium-alkyl hydroperoxides can be attributed to the fast and strong coordination of alcohol ligands to vanadium, followed by an intramolecular oxygen transfer from the coordinated alkyl peroxide to the double bond of the allylic alcohol. In Figure 1.5., the first step is the exchange of two alkoxide groups by the peroxide and the allylic alcohol; the next step, leading to **1,** is a bidentate coordination of the peroxide moiety. The alkene part of the allylic alcohol in **1** is lined up perpendicularly to the vanadium-alkylperoxo plane, making an interaction between the alkene and the peroxygen possible. This interaction is, from a frontier orbital point of view, similar to the interactions between alkenes and other transition metal-peroxo complexes. Steps **1** and **2** are the step in which the stereoselectivity is determined. With the mechanism outlined in Figure 1.5 for the epoxidation of allylic alcohols, the stereoselectivity for the formation of the *erythro*-epoxy alcohol can be explained from the conformation of the intermediate, see Figure 1.6a.
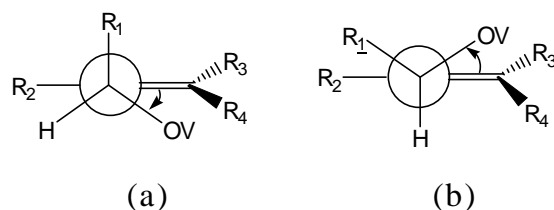
Figure 1.6. Structural diagram for (a) *erythro* and (b) *threo*.

The O-C-C=C dihedral angle $\emptyset$ [29] in Figure 1.6a is about 50^0, whereas a rotation of the O-C-C=C dihedral angle about 50^0 above the R_2,R_3,R_4 plane, shown in Figure 1.6b, will lead to the *threo* product. The substitution pattern supports the suggested conformations since alkyl substitution in R_1 and R_2 will cause steric repulsion in Figure 1.6b, whereas this is not the case in Figure 1.6a. The preferred orientation of the alkene part of the allylic alcohol perpendicular to the vanadium-alkylperoxo plane is very similar to the orientation of the allylic alcohol in titanium-tartrate catalyzed epoxidations. Ab initio calculations indicate a small (~ 1 kcal.mol^{-1}) preference for a planar orientation in the transition state; for these allylic alcohols an increase in the anionic character of the metal-oxygen bond, with its associated effect on the energy of the π bond, should increase the rate of epoxidation.

1.3. Literature reviews on the epoxidation of alkenes

Stereochemical control of the peracid epoxidation of olefins has been a subject of intense interest since the discovery of this reaction by Prileschajew in 1909. The mechanistic details of the oxygen transfer were described by Bartlett in terms of the ground-breaking planar "butterfly" transition state. The pioneering studies by Henbest label the first demonstration that the stereochemical course of the Prileschajew epoxidation may be steered through synergistic interplay between conformational and hydrogen-bonding effects (see Figure 1.7).
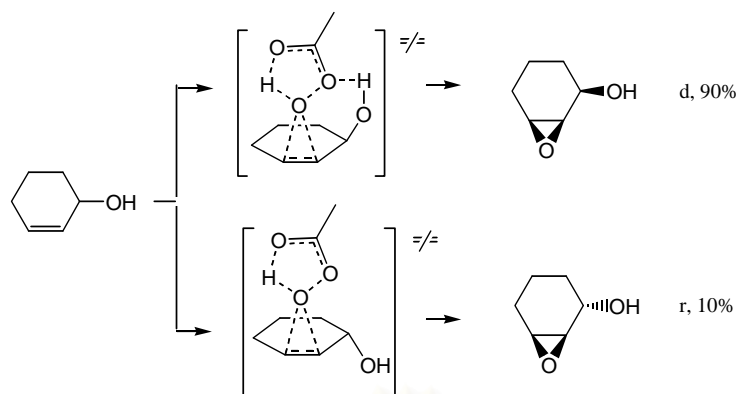
Figure 1.7. The transition structures of epoxidation thought hydrogen-bonding effects.

For 3-hydroxycyclohexene[30] it was shown that the cis epoxide was favored, which signifies that the perbenzoic acid attacks the π bond from the same side that bears the allylic alcohol functionality. That hydrogen bonding between the peracid and allylic alcohol substrate is responsible for the observed syn epoxidation (substrate control) was confirmed by the fact that on masking the hydroxy group in the form of methyl or acetyl derivatives then redominantly the trans epoxides were produced. The preferred anti attack of the peracid was rationalized in terms of steric effects since hydrogen bonding by the allylic substitutents with the peracid cannot apply.

In particular, the planar butterfly TS (Figure 1.8a), proposed several years ago by Henbest et al., has more recently been replaced by the spiro TS (Figure 1.8b). The transition structure (Figure 1.8c) was proposed later by Sharpless (in order to explain facial diastereoselectivities in the epoxidation of allylic alcohols) and has been widely accepted by organic chemists. In this model, the hydrogen bonding involves only the proximal peroxo oxygen in an exo spiro TS (i.e., the dihedral angle between the peroxy acid plane and the double bond plane is ~90°) with the plane of the peroxy acid moiety oriented at ~60° to the C=C bond axis (Figure 1.8d). Sharpless stressed that this geometrical array orients the front side lone pair to efficiently hydrogen bond with the allylic OH group while at the same time the second lone pair can interact favorably with the π^{*} orbital of the olefin (Figure 1.8e).
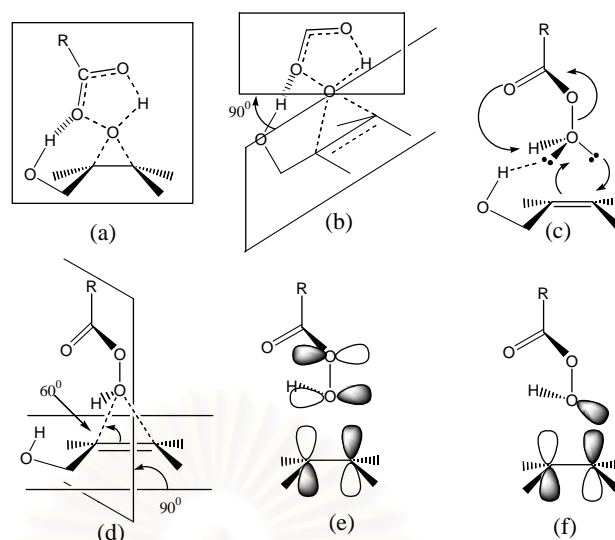
Figure 1.8. Qualitative models (c and d illustrate the Sharpless hypothesis) for transition structures of the epoxidation of allylic alcohols with peroxy acids. Schematic descriptions of the electron back-donation (HOMO peroxyformic – LUMO alkene) from peroxy acid to alkene (e and f).

W. Adam and A. K. Smerz[23] (1996) studied the solvent effects in the regio- and diastereoselective epoxidations of acyclic allylic alcohols by dimethyldioxirane. In hydrogen-bonding solvents (MeOH), the 6,7-epoxide is preferred over the 2,3-epoxide (74:26), which reveals that the more nucleophilic 6,7 double bond (the 2,3 double bond is inductively deactivated by the allylic hydroxy group) is preferentially attacked by the electrophilic dimethyldioxirane. In MeOH, regioisomeric dipolar transition states are equally well stabilized by interaction through intermolecular hydrogen bonding with solvent molecules. In the nonpolar CCl4, intramolecular hydrogen bonding with the allylic hydroxyl functionality favors to attack at the 2,3-double bond and proportionally more 2,3-epoxide is formed.

W. Adam et al.[31] (1999) prepared an epoxide with hexafluoroacetone perhydrate from chiral allylic alcohols to study regio- and diastereo-selective. They observed the threo diastereoselectivity with 1,3-allylic strain by hexafluoroacetone perhydrate and its regioselectivity in the epoxidation of 1-methylgeraniol establishes a hydroxy-directing effect through hydrogen bonding between the oxidant and the substrate. The higher syn selectivity for the cis than trans isomer of 5-*tert*-butylcyclohexen-3-ol suggests a hydrogen-bonded transition-state structure similar to that of peracids for this catalytic oxygen transfer process.

M. Freccero et al.[32] (1999) investigated the transition structures for epoxidations of allylic alcohols with peroxyformic acid to compete between peroxy acid oxygens as hydrogen bond acceptors in B3LYP. Syn attacks on these alcohols by peroxy acid lead to syn TSs in which hydrogen bonding is operative. The allylic OH group always acts as hydrogen-bond donor while either the carbonyl oxygen or the peroxo oxygens of the peroxy acid can play the role of hydrogenbond acceptors. In the case of propenol, the two syn TSs (Ø = 135.0° and 16.0°) with the peroxo oxygens involved in hydrogen bonding have free enthalpies comparable with those of their counterparts (Ø = 134.0° and 16.3°) with hydrogen bonding to carbonyl oxygen. Basis set extension as well as electrostatic solvation effects favor the former TSs over the latter ones. In the case of cyclobutenol the syn TS (Ø = 124.2°) with hydrogen bonding to peroxo oxygens is significantly more stable (by 1.8 kcal/mol^{-1}) than the corresponding TS (Ø = 128.0°) with carbonyl oxygen involved in hydrogen bonding. Anti TSs are inherently less stable than syn TSs but this difference is strongly reduced in solution.

M. Freccero et al.[33] (2000) investigated the transition structures in epoxidation with peroxy acids. They observed the geometry of all TSs substantially conforms to a spiro butterfly orientation of the reactants while no TS resembles the planar butterfly structure. However theoretical *threo*:*erythro* epoxide ratios accord with experimental data. Calculations indicate that *threo* epoxides derive mostly from TSs in which the olefinic OH assumes an outside conformation while *erythro* epoxides originate from TSs with the OH group in an inside position. Computational findings do not support the qualitative TS models recently proposed for these reactions.

R. D. Bach et al.[34] (1998) reported the origin of substrate directing effects in the epoxidation of allyl alcohols with peroxyformic acid. The free energy of activation ($\Delta G^{\ddagger}$) 19.8 kcal/mol) predicted at the MP4/6-31G(d)//MP2/6-31G(d) level is quite comparable with experimental data for epoxidation of 3-hydroxycyclohexene ($G^{\ddagger}_{278}$= 19.7 kcal/mol). A spiro transition state (TS) was found where the plane defined by the peroxyacid moiety is oriented at 89° to the C=C bond axis. Intrinsic reaction coordinate analysis suggests that after the barrier is crossed a 1,4-hydrogen migration of the peroxyacid hydrogen to the carbonyl oxygen takes place in concert with O-O bond cleavage affording the epoxide of allyl alcohol hydrogen bonded to the neutral formic acid leaving group. The activation parameters calculated at the B3LYP/6-311G(d,p) level are in excellent agreement with the MP4//MP2 values. The

transition structure with the allyl alcohol O-C-C=C dihedral angle of 16.4° is 2.1 kcal/mol lower in energy than a transition structure with a dihedral angle of 134.3°. The directing effect of the hydroxyl group is attributed initially to a primary hydrogen bonding interaction between the relatively more acidic peroxy acid proton and the oxygen of the allyl alcohol.

K. N. Houk et al.[35] (1997) studied the transition structures for the epoxidations of ethylene by performic acid, dioxirane, oxaziridine, and peroxynitrous acid. All of the epoxidations have spiro transition states; those with performic acid and dioxirane are the involve synchronous oxygen transfer, while those with oxaziridine and peroxynitrous acid are later with asynchronous oxygen transfer. The results from B3LYP/6-31G* theory are compared with MP2/6-31G* literature values. Substitution on ethylene by methoxy, methyl, vinyl, and cyano groups changes the transition state geometries toward asynchronous spiro structures. The activation energies are lowered by all substituents except the cyano group in reactions of performic acid and dioxirane. Experimental stereoselectivities are rationalized by using transition structure models based upon these transition structures.

W. Adam et al.[36] (1999) catalyzed the epoxidation of chiral allylic alcohols by manganese(salen) and iron(porphyrin) complexes to compare regio- and diastereoselectivity. Their discussion presented the dihedral angle O-C-C=C (R) between the π plane of the double bond and the hydroxy group of the allylic system optimal dihedral angles (O-C-C=C) have been estimated to be 100-115° for manganese(salen) and Iron(porphyrin) complexes (Figure 1.9a,b), 40-50° for VO(acac)$_2$/TBHP (Figure 1.9c), 70-90° for Ti(Oi-Pr)$_4$/TBHP (Figure 1.8d), 120° for m-CPBA (Figure 1.8e), and 130° for DMD (Figure 1.8f) to rationalize the observed diastereoselectivities.
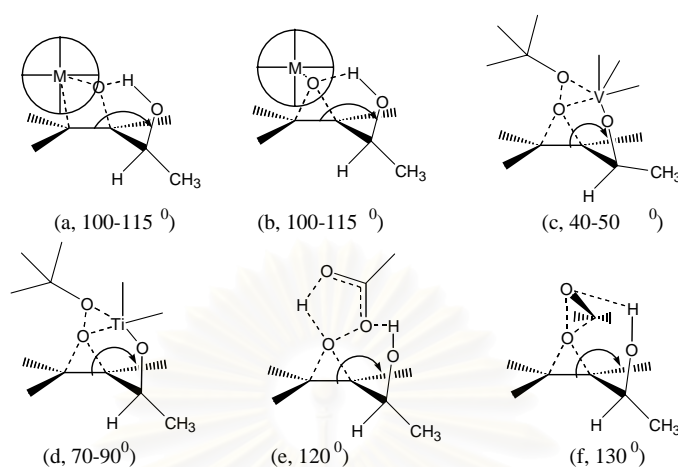
Figure 1.9. Transition-state structures for the epoxidation catalyzed by the manganese (salan) and iron (porphine) complexes (a,b), VO(acac)$_2$/TBHP (c), Ti(O^{t}Pr)$_4$/TBHP (d), *m*-CPBA (e), and DMD (f).

W. Adam et al.[37] (2000) investigated the *threo* diastereoselectivity of muti-pathway of epoxidation. The contribution of the four lowest energy transition structures to the *threo*:*erythro* product ratio has been assessed through an extended Curtin-Hammet principle analysis of this multi-transition state reaction. It has been found that this approach agrees well with the experimental *threo*:*erythro* product ratio, in particular when the corrections for a solvent effect are made within the self-consistent isodensity polarized continuum model (SCI-PCM).

W. Adam et al.[38] (2002) investigated the *threo*:*erythro* product ratios of epoxidation from three chiral allylic alcohols by the density-functional theory method, B3LYP/6-31+G(d,p). and compared with experiment. For each substrate we calculated the two prereaction complexes with Ti(OH)$_4$/MeOOH (the oxidant model for Ti(O-*i*-Pr)$_4$/*t*-BuOOH), their *threo* and *erythro* transition states for oxygen transfer, and the corresponding product complexes. The diastereoselectivity of this diastereoselective oxyfunctionalization is rationalized in terms of the competition between 1,3A and 1,2A strain and the electronic advantage for the spiro transition state.

W. Adam et al.[39] (2003) prepared and analyzed epoxides with control of enantioselectivity through a hydrogen-bonded template in the vanadium(V)-catalyzed

by optically active hydroperoxides. From this mechanistic study they conclude that this novel enantioselective oxygen transfer takes place via a hydrogen-bonded template, held together by the vanadium metal.

R. Zhang et al.[40] (2003) used Sandwich-type polyoxometalates (POMs), $[WZnM_2(ZnW_9O_{34})_2]^{q-}$ [M) Mn(II), Ru(III), Fe-(III), Pd(II), Pt(II), Zn(II); q=10-12], are shown to catalyze selectively the epoxidation of chiral allylic alcohols with 30% hydrogen peroxide under mild conditions (ca. 20°C) in an aqueous/organic biphasic system. The transition metals M in the central ring of polyoxometalate do not affect the reactivity, chemoselectivity, or stereoselectivity of the allylic alcohol epoxidation by hydrogen peroxide. Similar selectivity, albeit in significantly lower product yields are observed for the lacunary Keggin POM $[PW_{11}O_{39}]^{7-}$, in which a peroxotungstate complex has been shown to be the active oxidizing species. Their discussion proposed the dihedral angle O-C-C=C (R) between the π plane of the double bond and the hydroxy group of the allylic system optimal dihedral angles (O-C-C=C) have been estimated to be 50-70° for POM/H_2O_2 (Figure 1.10c) and compared VO(acac)$_2$/TBHP (Figure 1.10a), Ti(OiPr)$_4$/TBHP (Figure 1.10b).
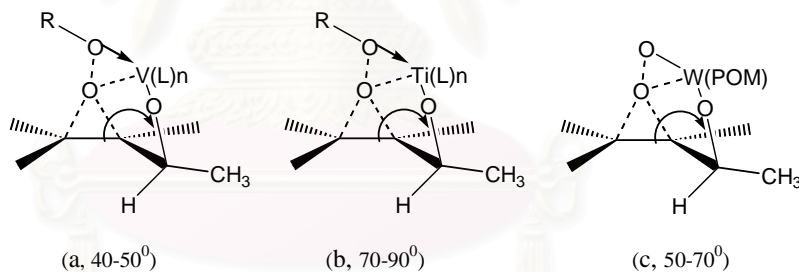
Figure 1.10. Proposed transition structures with the optimal dihedral angles for the epoxidation of allylic alcohols by compared VO(acac)$_2$/TBHP (a), Ti(OiPr)$_4$/TBHP (b) and POM/H_2O_2 (c).

R. D. Bach et al.[41] (2003) compared analysis of the calculated gas-phase activation barriers for the epoxidation of ethylene with dimethyldioxirane (DMDO) and peroxyformic acid (PFA). Competition experiments in CH_2Cl_2 solvent reveal that DMDO reacts with cyclohexene much faster than peracetic acid/acetic acid under scrupulously dried conditions. The rate of DMDO epoxidation is catalyzed by acetic acid with a reduction in the classical activation barrier of 8 kcal/mol. The thermodynamic stability of DMDO is largely a consequence of the combined geminal

dimethyl- and dioxa-substitution effects and unusually strong C-H and C-CH$_3$ bonds. ethyl(trifluoromethyl) dioxirane (TFDO) exhibits much lower calculated activation barriers than DMDO in the epoxidation reaction.

P. E. Sinclair et al.[13] (1999) studied quantum of the mechanism of partial oxidation reactivity in titanosilicate catalysts within the cluster approximation. Results using the BP86 functional and a DZVP basis suggest that, on interaction with hydrogen peroxide, a titanium bidentate-peroxide species, Ti(η_2-OOH) is formed, which then donates an oxygen to a weakly bound alkene molecule. Their calculated estimate of the activation barrier for oxidation, in good agreement with experiment, is around 70 kJ mol^{-1}, depending on the route followed. A mechanism for alkene oxidation over Ti^{IV}-silica catalysts in the presence of hydroperoxides is proposed, consistent with available experimental and theoretical data and including the effects on the reaction of different solvents, peroxides, additives, and bases.

R. R. Sever et al.[42] (2003) compared epoxidation and Baeyer-Villiger reaction pathways for Ti(IV)-H$_2$O$_2$ and Sn(IV)-H$_2$O$_2$ by modeled with unconstrained single coordination sphere clusters using a B3LYP/ECP methodology. Activation of hydrogen peroxide via formation of a metal hydroperoxo intermediate proceeds with similar energetic over titanium and tin. The overall reaction kinetics for epoxidation of either ethylene or 2,3-dimethyl-1-butene are also similar for Ti(IV)-H$_2$O$_2$ and Sn(IV)-H$_2$O$_2$. The intrinsic reaction rate for Baeyer-Villiger oxidation of either acetone or 2-methyl-3-pentanone is approximately 5 orders of magnitude slower with Ti(IV)-H$_2$O$_2$ than with Sn(IV)-H$_2$O$_2$.

H. Munakata et al.[43] (2001) showed possibility to form the hydrated peroxotitano-silicalite complex, containing a (Ti)-O-O-(Si) peroxo-moiety, as an oxidizing agent. Using this hydrated peroxo-titanosilicalite complex as an oxidizing agent, oxidation mechanisms were postulated for ethane epoxidation and for ammonia oxidation to form hydroxylamine. They used a cluster model of a titanosilicate catalyst to calculate an activation of hydrogen peroxide by density functional theory.

T. Kudo a et al.[44] (2003) investigated the catalytic reactivity of titanosilsesquioxanes and titanosiloxanes with *ab initio* electronic structure theory including electron correlation effects. The reactions examined are the oxidation of olefins and polymerization of ethylene. The titanium compounds are found to be promising effective catalysts for the oxidation reactions, with the catalytic activity increasing with the number of Ti-containing substituents. Ring and cage structures

also enhance the catalytic ability of these compounds, whereas the addition of Si containing substituents has the opposite effect. The same Ti compounds are predicted to be less effective as catalysts for ethylene polymerization.

1.4. Objective of the present study

The diastereoselectivity of epoxidation have important to synthesis the syntactic polymer and some material. For to describe the reason of selectivity, the objectives of this thesis are:

(i) To study the pathway of epoxidation by transition-metal catalyzed complex/ hydrogenperoxide,

(ii) To study the structure and orientation of the transition state of vanadium complex in epoxidation,

(iii) To evaluate the *threo:erythro* product ratio of epoxidation.

CHAPTER II

THEORY AND METHOD OF CALCULATION

The computational chemistry is concerned with the calculating and predicting the properties of atomic and molecular systems. It is based on the fundamental laws of quantum mechanics and uses a variety of mathematical transformation and approximation techniques to solve the fundamental equations.

2.1. Quantum mechanics

Quantum mechanics was formulated independently by Erwin Schrödinger and Werner Heisenberg in 1925. Schrödinger's method is formulated in terms of the partial differential equations used to describe waves. Heisenberg's method used matrices and at first glance appears very different from Schrödinger's. It was shown, however, that the two ways are mathematically equivalent. Chemistry customarily uses the wave mechanics method to develop its treatment of quantum mechanics.

The solutions to the Schrödinger equation are called wave functions and these wave functions give a complete description of any system. The Schrödinger equation can not be derived, instead it is postulated that is assumed to be true for the purposes of our reasoning. It is in fact the fundamental postulate of quantum mechanics.

2.1.1. Time-independent Schrödinger equation

The problems in quantum mechanics are usually concerned with many-electron system which it deals with the time-independent Schrödinger equation. The time-independent Schrödinger equation is

$$\hat{H}\Psi = E\Psi \tag{2.1}$$

Where $\hat{H}$ is the Hamiltonian operator, representing all contributions of energies in the system. E is the total energy of the system. The wavefunction, Ψ, is a function of

the electronic and atomic nuclei coordinates that describes the considerate system. In atomic units, the Hamiltonian for n electrons and M nuclei is the summation of kinetic energy operator and potential energy operator.

$$\hat{H} = \hat{T} + \hat{V} \tag{2.2}$$

$\hat{T}$ represents the summation of kinetic energy operator of electron and atomic nuclei,

$$\hat{T} = -\frac{1}{2}\sum_{i=1}^{n}\nabla_i^2 - \frac{1}{2m_A}\sum_{A=1}^{M}\nabla_A^2 \tag{2.3}$$

The differential operator "del squared" in equation 2.3 is known as Laplacian operator. The operator del is equivalent to partial differentiation with respect to x, y and z components.

Where as; $\nabla^2 is \dfrac{\partial^2}{\partial x^2} + \dfrac{\partial^2}{\partial y^2} + \dfrac{\partial^2}{\partial z^2}$ or $\dfrac{1}{r^2}\dfrac{\partial}{\partial r}\left(r^2\dfrac{\partial}{\partial r}\right) + \dfrac{1}{r^2\sin\theta}\dfrac{\partial}{\partial\theta}\left(\sin\theta\dfrac{\partial}{\partial\theta}\right) + \dfrac{1}{r^2\sin^2\theta}\dfrac{\partial^2}{\partial\phi^2}$

for in Cartesian and polar coordinates, respectively. $\hat{V}$ presents the potential energy operator consist of nuclei-electron attraction, electron-electron repulsion and nuclei-nuclei repulsion.

$$\hat{V} = -\sum_{i=1}^{n}\sum_{A=1}^{M}\frac{Z_A}{r_{iA}} + \sum_{i=1}^{n}\sum_{j>i}^{n}\frac{1}{r_{ij}} + \sum_{A=1}^{M}\sum_{B>A}^{M}\frac{Z_A Z_B}{R_{AB}} \tag{2.4}$$

2.1.2. The Born-Oppenheimer approximation

The Born-Oppenheimer approximation is the first of several approximations used to simplify the solution of the Schrödinger equation. From this approximation, it can consider the molecular problem by separating nuclear and electronic motions. It is reasonable since the mass of nuclei is much greater than an electron. Thus, the electrons can move much faster than the nuclei, and the electron reacts essentially instantaneously to change in nuclear position. Therefore the electron distribution within a molecular system depends on the positions of the positions of the nuclei, and

not on their velocities. The electronic motions in molecular system are moving in the potential generated by the field of stationary nuclei. In this condition, the Hamiltonian operation is constructed by omitting the nuclear kinetic energy term.

$$\hat{H}_{elec} = -\frac{1}{2}\sum_{i=1}^{n}\nabla_i^2 - \sum_{i=1}^{n}\sum_{A=1}^{M}\frac{Z_A}{r_{iA}} + \sum_{i=1}^{n}\sum_{j>i}^{n}\frac{1}{r_{ij}} + \sum_{A=1}^{M}\sum_{B>A}^{M}\frac{Z_A Z_B}{R_{AB}} \qquad (2.5)$$

This Hamiltonian operator is used in the Schrödinger equation describing the motion of electrons in the field of fixed nuclei.

$$\hat{H}_{elec}\psi_{elec}(r,R_A) = E_{eff}(R_A)\psi_{elec}(r,R_A) \qquad (2.6)$$

Solving this equation for the electronic wavefunction will be produced the effective nuclear potential function, $E_{eff}(R_A)$. This potential function depends on the nuclear coordinated and describes the potential energy surface for the system.

$$\hat{H}_{nucl} = \hat{T}_{nucl}(R_A) + E_{eff}(R_A)$$

(2.7)

This equation is used for nuclear motion, describing the vibrational, rotational and translational state of the nuclei. Solving the nuclear Schrödinger equation is necessary for predicting the vibration spectra of molecules.

2.1.3. Antisymmetry of the wavefunction on exchange of two electrons

In systems with more than one electron a fundamental problem arises as we cannot distinguish between the electrons and cannot specify position and linear momentum at the same time and thus cannot follow electron trajectories. In other words, quantum mechanics must still predict the same expectation values for all observables when interchanging the coordinates (three space coordinates and spin coordinate) of two electrons. For all possible values of the coordinates, this means that the two wavefunctions must be the same, except for their phase. In other words, the exchange of the coordinates of two electrons can only result in a phase shift of the wavefunction.

Wavefunction, in a system consisting of more than one particle, respect to interchange of two particles, the wavefunction can be either symmetric or antisymmetric. A quantum-mechanical treatment of the helium atom agrees the wavefunction must be antisymmetric with respect to exchange of two electrons. Furthermore, by postulating that wavefunctions in many-electron systems are generally antisymmetric with respect to exchange of two electrons can derive the Pauli principle. This requirement for antisymmetry is therefore a generalization of the Pauli principle.

2.1.4. Slater determinants

In 1929 Slater recognized that determinants provide a simple means of ensuring the antisymmetry of a wavefunction. An exchange of two electrons in a 2 spin orbitals can be written as

$$\Psi = \frac{1}{\sqrt{n!}} \begin{vmatrix} \psi_1(x_1)\alpha(1) & \psi_1(x_1)\beta(1) & \psi_2(x_1)\alpha(1) & \cdots & \psi_{\frac{n}{2}}(x_1)\beta(1) \\ \psi_1(x_2)\alpha(2) & \psi_1(x_2)\beta(2) & \psi_2(x_2)\alpha(2) & \cdots & \psi_{\frac{n}{2}}(x_2)\beta(2) \\ \vdots & \vdots & \vdots & & \vdots \\ \psi_1(x_n)\alpha(n) & \psi_1(x_n)\beta(n) & \psi_2(x_n)\alpha(n) & \cdots & \psi_{\frac{n}{2}}(x_n)\beta(n) \end{vmatrix} \quad (2.8)$$

Where $\psi_i(x_n)$ are the wavefunctions of n electrons, doubly occupying $\frac{n}{2}$ orbitals.

The spin functions, α and β are orthonormal. The pre-factor $\frac{1}{\sqrt{n!}}$ normalizes the Slater determinant. This determinant mixes all of the possible orbitals of electrons in the molecular system to form the wavefunction.

2.1.5. Basis set

Basis set is a set of functions used to describe the shape of the orbitals in an atom. There are two types of basis functions, Slater type orbitals (STO) and Gaussian type orbital (GTO), commonly used in Electronic structure calculations:

Slater type orbitals have the function form

$$\chi_{\varsigma,n,l,m}(r,\theta,\varphi) = NY_{l,m}(\theta,\varphi)r^{(n-1)}e^{-\varsigma} \tag{2.9}$$

N is a normalization constant and $Y_{l,m}$ are the usual spherical harmonic functions. The exponential depend on the distance between the nucleus and electron.

There are two guidelines for choosing the basis function one is that should have behavior which agrees with the physics of problem electron between the nucleuses becomes large. Two is the chosen functions should make it easy to calculate all the required integrals. The first criterion suggests the use of exponential functions located on the nuclei; such functions are known to be exact solutions for the hydrogen atom.

Gaussian type orbital can be written in term of polar or Cartesian coordinates.

$$\chi_{\varsigma,n,l,m}(r,\theta,\varphi) = NY_{l,m}(\theta,\varphi)r^{(2n-2-1)}e^{-\varsigma^2} \tag{2.10}$$

$$\chi_{\varsigma,n,l,m}(x,y,z) = NY_{l,m}x^{l_x}y^{l_y}z^{l_z}e^{-\varsigma} \tag{2.11}$$

The r^2 dependent on the exponential makes the GTO inferior to the STOs in two aspects.

(1) At the nucleus GTO has a zero slope, in contrast the STO has a "curp"(discontinuous derivative), and GTOs have problem representing the proper behaviors near the nucleus.

(2) The GTO falls off too rapidly far from the nucleus compared with the STO, and the "tail" of the wave function is consequently represented poorly.

Three- and four-center integrals are very difficult if the atomic orbitals are based on different atoms. Gaussian functions are computationally much easier to handle.

This is because the product of two function Gaussian function located at two different positions (R_A+R_B) with different exponentials (α and β) can be written as a single Gaussian located intermediately between the two original positions. This allows compact formulas for all type of one and two-electron integrals to be derived.

$$G_A(r) = \left(\frac{2\alpha}{\pi}\right)^{3/4}e^{-\alpha(r-R_A)^2} \tag{2.12}$$

$$G_B(r) = \left(\frac{2\beta}{\pi}\right)^{3/4} e^{-\beta(r-R_B)^2} \tag{2.13}$$

$$G_B(r)G_A(r) = Ke^{-\gamma(r-R_c)^2} \tag{2.14}$$

Where $\gamma = \alpha + \beta$, $\quad R_c = \dfrac{\alpha R_A + \beta R_B}{\alpha + \beta}$, $\quad K = \left(\dfrac{2}{\pi}\right)^{3/2} (\alpha\beta)^{3/4} e^{-\frac{\alpha\beta}{\alpha+\beta}(R_A-R_B)^2}$.

$$\exp(-\alpha_m r_m^2)\exp(-\alpha_n r_n^2) = \exp\left(-\frac{\alpha_m\alpha_n}{\alpha_m+\alpha_n} r_{mn}^2\right)\exp(-\alpha\ r_c^2) \tag{2.15}$$

r_{mn} is the distance between the centers m and n and the orbital exponential α of the combined function is related to the exponential α_m and α_n by

$$\alpha = \alpha_m + \alpha_n$$

Minimal basis sets

The simplest level of *ab initio* molecular orbital theory involves the use of a minimal basis set of nuclear-centered functions. In the strictest sense, such a representation comprises exactly that number of functions required to accommodate all of the electrons of the atom, while maintaining overall spherical symmetry. For example, within framework of a minimal basis set, hydrogen and helium are represented by a single s-type function, lithium and belyllium by a pair of such functions, and the remaining first-row elements (boron to neon) by two s functions and a complete set of three p-type functions.[45] Several methods exist to form contracted Gaussians sets. Minimal CGTF sets are often formed by fitting STOs. One starts with a minimal basis set of one STO per AO with the STO orbital exponents fixed at values found to work well in calculations on small molecules. Each STO is then approximated as a linear combination of *N*. Gaussian functions, where the coefficients in the linear combination and the Gaussian orbital exponents are chosen to give the best least-squares fit to the STO. Most commonly, *N*=3, giving a set of CGTFs called STO-3G; this basis set is defined for the atoms H through Xe. Since a linear combination of three Gaussian is only an approximation to an STO, the STO-3G basis set gives results not quite as good as a minimal basis-set STO calculation. A minimal basis setoff STOs for a compound containing only first-row elements and hydrogen is denoted by (2*s*1*p*/1*s*). Since each STO is replaced by a linear combination of three primitive Gaussians, the STO-3G basis set for compound of first-row atoms and H is

denoted by (6s3p/3s) contracted to [2s1p/1s], where parentheses indicate the primitive Gaussians and brackets indicate the contracted Gaussians.[46]

Extended *sp* basis sets

Minimal basis sets have several inherent inadequacies. Because the number of atomic basis functions is not apportioned according to electron count-for example, the lithium atom, which has only three electrons, is provided with the same number of functions (five) as fluorine with its nine electrons-it follows that minimal basis set descriptions of compound containing elements such as oxygen and fluorine are likely to be poorer than those for molecules comprising elements with fewer electrons. A second problem arises because a minimal basis set using fixed Gaussian exponents is unable to expand and contract in response to differing molecular environments. This is because a minimal basis set contains only a single valence function of each particular symmetry type, for example 2s, 2px. Thus, in the absence of radial exponent optimization for each atom in a molecule, there is no mechanism for the individual sets of functions to adjust their sizes. Finally, minimal representations lark the ability to describe adequately the non-spherical anisotropic aspects of molecular charge distributions.[45]

The 6-31G* basis set is a valence double-zeta polarized basis set that adds to the 6-31G set six d-type Cartesian-Gaussian polarization functions on each of the atoms Li through Ca and ten *f*-type Cartesian-Gaussian polarization functions on each of the atoms Sc through Zn. 6-31G** basis set adds to the 6-31G* set a set of three *p*-type Gaussian polarization functions in these two basis set were determined as the average of the optimum values found in calculations on small molecules.[46]

In principle, the first two deficiencies may be alleviated simply by allowing for more than a single valence function of each symmetry type in the basis set description. In this way, the number of basis functions for all elements, not just those on the left-hand side of the Periodic Table, would be substantially in excess of the number actually required. Furthermore, the allocation of two or more valence basis functions of each given symmetry type would provide the needed flexibility for overall radial size to be determinate simply by the adjustment of the relative weights of the individual components in the variation procedure.

The third deficiency, the inability of a minimal basis set to describe properly anisotropic molecular environments, may be alleviated in one of two ways. The conceptually simpler way would be to allow each of the x, y and z p components

describing the valence region of a main group element to have different radial distribution, that is to employ an anisotropic rather than an isotropic minimal basis set. Similarly, the five d-function components describing the valence manifold of a first- or second-row transition metal could be independently specified.

A basis set formed by doubling all functions of a minimal representation is usually termed a double-zeta basis. An even simpler extension of a minimal basis set is to double only the number of basis functions representing the valence region.

2.1.6. The variation method

The variational principle is an important approach to find approximate solution to Schrödinger's equation. It states that the expectation value or average value of the energy for an approximation wave function always lies above or equal the exact solution of Schrödinger equation for the same Hamiltonian operator. This means that if there are trial wave functions that contains adjustable parameters and minimize the expectation value of the energy, then approaching the exact result.

The expectation value or average value of the energy, E_a can be calculated by

$$\langle E \rangle = \frac{\int \psi_a^* \hat{H} \psi_a d\tau}{\int \psi_a^* \psi_a d\tau} = \frac{\langle \psi_a | \hat{H} | \psi_a \rangle}{\langle \psi_a | \psi_a \rangle} \tag{2.16}$$

The trial wave function can be expressed in terms of a linear combination of the exact eigenfunctions of ψ_i

$$\psi_a = \sum_i c_i \psi_i \tag{2.17}$$

Now consider the integral

$$\int \psi_a^* (\hat{H} - E_0) \psi_a d\tau = \sum_i \sum_v c_i^* c_v \int \psi_i^* (\hat{H} - E_0) \psi_v d\tau$$

$$= \sum_i \sum_v c_i^* c_v (E_i - E_0) \int \psi_i^* \psi_v d\tau$$

$$= \sum_i c_i^* c_i (E_i - E_0) \geq 0 \qquad (2.18)$$

Since the E_0 is the lowest eigenvalue, $E_i - E_0$ can never be negative. The quantity of $c_i^* c_i$ is always positive or zero $\left(|c_i|^2 \geq 0 \right)$ and $E_i \geq E_0$, hence,

$$\int \psi_a^* (\hat{H} - E_0) \psi_a d\tau \geq 0 \qquad (2.19)$$

from which follows the variational principle which states that for a trial wavefunction ψ, the energy, E, computed as the expectation value of the Hamiltonian is an upper bound to the exact ground state energy, E_0, (i.e. $E_a - E_0$). This also gives insight into how to and the best approximate wavefunctions, as

$$E_a = E_0 \Leftrightarrow \psi_a = \psi_0 \qquad (2.20)$$

Therefore, minimization of the energy, E_a, with respect to all allowed variable parameters in ψ_a will give the best ground state energy and wavefunction. This is the most important result.

2.2. The Hartree-Fock equations

The Hartree-Fock theory considers the single determinant formed from electrons' orbital as the best possible approximation to the ground state of the N-electron system described by an electronic Hamiltonian $\hat{H}$. The variation principle states that if a normalized wavefunction $\left| \tilde{\phi} \right\rangle$ that satisfies the appropriate boundary conditions is given, the expectation value of the Hamiltonian is an upper bound to the exact ground state energy. That is, if $\left\langle \tilde{\phi} \middle| \tilde{\phi} \right\rangle = 1$ then

$$\left\langle \tilde{\phi} \middle\| \tilde{\phi} \right\rangle \geq \mathrm{E}o \tag{2.21}$$

The equality holds only when $\left| \tilde{\phi} \right\rangle$ is identical to the exact wavefunction. The problem of minimizing a function subject to a constraint of normalization is solved by Lagrange's method of undetermined multipliers. According to the variational principle, the best orbitals are those which minimize the electronic energy E, which is defined by

$$\mathrm{E} = \left\langle \psi \middle| \hat{H} \middle| \psi \right\rangle$$

$$= \sum_{\alpha}^{N} \left\langle \alpha \middle| \hat{h} \middle| \alpha \right\rangle + \frac{1}{2} \sum_{\alpha\beta}^{N} \left(\left\langle \alpha\beta \middle| \alpha\beta \right\rangle - \left\langle \alpha\beta \middle| \beta\alpha \right\rangle \right) \tag{2.22}$$

$$= \sum_{\alpha}^{N} h_{\alpha\alpha} + \frac{1}{2} \sum_{\alpha\beta}^{N} (J_{\alpha\beta} - K_{\alpha\beta})$$

Where $\hat{h}$ is a core-Hamiltonian for an electron, describing its kinetic energy and potential energy in the field of the nuclei and $J\alpha\beta$ and $K_{\alpha\beta}$ is the coulombic energy and exchange energy, respectively. By a linear variational method, the orbitals can be systematically varied with the constraint that they remain orthonormal until the energy E_0 is a minimum.

For a given single determinant $\left| \psi \right\rangle \equiv \left| \phi_1 \phi_2 .... \phi_n \right\rangle$ the energy is a function of the orbitals (ϕ_i). To minimize E with respect to the orbital, subject to the contain that the orbitals remain orthonormal.

$$\int dx(1)\phi_a^* \phi_b(1) = \left\langle \phi_a \middle| \phi_b \right\rangle = \delta_{ab} \tag{2.23}$$

Using the variation principle, the best orbitals that minimize E are obtained from

$$\left[\hat{h}(1) + \sum_{b=1}^{N} \hat{J}_b(1) - \hat{K}_b(1) \right] \phi_a(1) = \sum_{b=1}^{N} \varepsilon_{ab} \phi_b(1) \tag{2.24}$$

The coulombic operator, corresponding to the classical electrostatic interaction, is defined by

$$\hat{J}_b(1)\phi_a(1) = \left[\int dx_2 \phi_b^*(2) r_{12}^{-1} \phi_b(2)\right]\phi_a(1) \tag{2.25}$$

and the non-local potential operator describing the exchange term is defined by

$$\hat{K}_b(1)\phi_a(1) = \left[\int dx_2 \phi_b^*(2) r_{12}^{-1} \phi_a(2)\right]\phi_b(1) \tag{2.26}$$

Eq. (2.24) can be written in a short from of

$$\hat{F}|\phi_a\rangle = \sum_{b=1}^{N} \varepsilon_{ba}|\phi_b\rangle \tag{2.27}$$

The Fock operator, $\hat{F}$, is an effective one-electron operator, describing the kinetic energy of an electron, the attraction of all the nuclei and the repulsion of all the outer electrons (via $\hat{J}$ and $\hat{K}$ operators) called the Fock operator, of the from

$$\hat{F}(1) = \hat{h}(1) + \sum_{b=1}^{N} \hat{J}_b(1) - \hat{K}_b(1) \tag{2.28}$$

Eq. (2.27) is not in the canonical eigenvalue form. The reason is that any single determinant wavefunction formed from a set of orbital retains a certain degree of flexibility in the orbitals. It is always possible to find a unitary matrix U such that the transformation diagonalizes. A new set of orbital $\{\phi_a'\}$ can be obtained from an old set $\{\phi_a\}$ by a unitary transformation, $\phi_a' = \sum_b \phi_b U_{ba}$ Then Eq. (2.27) can be written in the canonical eigenvalue form without changing the expectation value of energy.

$$\hat{F}|\phi_a'\rangle = \varepsilon_a|\phi_a'\rangle \tag{2.29}$$

Where ε_a is the orbital enegy of ϕ'_a from Eq. (2.22) the total electronic energy E is given by

$$E = \sum_{a}^{N} \frac{1}{2}(h_{aa} + \varepsilon_a) \qquad (2.30)$$

Since the Fock operator has a functional dependence, through the Coulomb and exchange operators, on the solution of $\{\phi_i\}$ of the pseudo-eigenvalue equation, thus the Hartree-Fock equations are really nonlinear equations and will need to be solved by iterative procedures.

2.3. Density functional theory

According to the density functional theory proposed by Hohenberg and Kohn in 1964, the total energy of a system at the ground-state can be expressed as a functional of the electron density. Moreover, every observations of a stationary quantum mechanical system can be calculated from the ground-state density alone, while the ground-state density can be calculated using the variational method. However, for the time being, it seems that there is no way to avoid wavefunctions in molecular calculations and for accurate calculations they have to be used as a mapping step between the energy (and other observations) and the electron density. DFT has come to prominence over the last decade as a potentially capable method of very accurate results at low cost. Parr and Yang, 1994 in practice, approximations are required to implement the theory, and a significantly variable accuracy results. Calibration studies are therefore required to establish the likely accuracy in a given class of systems.

2.3.1. The Hohenberg-Kohn theorem

Within a Born-Oppenheimer approximation, the ground state of the system is a result of the positions of the nuclei. In the quantum mechanics hamiltonian equation 2 the kinetic energy of electrons ($\hat{T}_e$) and the electron-electron interaction ($\hat{V}_{ee}$) adjust themselves to the external potential ($\hat{V}_{ext}$) to get the lowest total energy. Thus, the external potential can be uniquely determined from knowledge of the electron density.

The Hohenberg-Kohn theorem states that if N interacting electrons move in an external potential V_{ext}, the ground-state electron density $\rho_0(r)$ minimizes the functional

$$E[\rho] = F[\rho] + \int \rho(r) V_{ext}(r) dr \tag{2.31}$$

In Eq. 2.31 $F[\rho]$ is a universal functional of $\rho(r)$ and the minimum value of the functional E is E_0, the exact ground-state electronic energy and by using the variation principle, the density can be obtained.

$$\hat{F} = \hat{T}_e + \hat{V}_{ee} = \sum_i -\frac{1}{2}\nabla_i^2 + \sum_{i \neq j} \frac{1}{|r_i - r_j|} \tag{2.32}$$

2.3.2. DFT exchange and correlations

The form of E_{XC} is in general unknown and its exact value has been calculated for only a few very simple systems. In the density functional theory, the exchange energy is defined as

$$E_X[\rho] = \langle \phi[\rho] | \hat{V}_{ee} | \phi[\rho] \rangle - U[\rho] \tag{2.33}$$

When $U[\rho]$ is the Hartree piece of the coulombic potential. The correlation term is defined as the remaining unknown piece of the energy:

$$E_C[\rho] = F[\rho] - T_s[\rho] - U[\rho] - E_X[\rho] \tag{2.34}$$

Due to the definition of $F[\rho]$, the correlation energy consists of two separate contributions:

$$E_C[\rho] = T_C[\rho] + U_C[\rho] \tag{2.35}$$

When $T_C[\rho]$ and $U_C[\rho]$ are the kinetic contribution and the potential contribution, respectively, of the correlation energy.

In electronic structure calculations, E_{XC} is most commonly approximated within the local density approximation or generalized-gradient approximation. In the local density approximation (LDA), the value of $E_{xc}[\rho(r)]$ is approximated by the exchange-correlation energy of an electron in homogeneous electron gas of the same density $\rho(r)$, *i.e.*

$$E_{XC}^{LDA}[\rho(r)] = \int \epsilon_{XC}(\rho(r))\rho(r)dr \qquad (2.36)$$

The most accurate data for $\epsilon_{XC}(\rho(r))$ is calculated from Quantum Monte Carlo calculations. For systems with slowly varying charge densities this approximation generally gives very good results. An obvious approach to improving the LDA, so called generalized gradient approximation (GGA), is to include gradient corrections by making E_{XC} a functional of the density and its gradient:

$$E_{XC}^{GGA}[\rho(r)] = \int \epsilon_{XC}(\rho(r))\rho(r)dr + \int F_{XC}[\rho(r),|\nabla\rho(r)|]dr \qquad (2.37)$$

Where F_{XC} is a correction chosen to satisfy one or several known limits for E_{XC}. Clearly, there is no unique recipe for the F_{XC}, and several functionals have been proposed in the literature.

2.3.3. Hybrid functional

From the Hamiltonian equation and the definition of the exchange-correlation energy, an exact connection can be made between the E_{xc} and the corresponding potential connecting the non-interacting reference and the actual system. The resulting equation is called the ACF -- Adiabatic connection formula and involves an integration over the parameter λ which turns on the electron-electron interaction

$$E_{XC} = \int_0^1 \langle \psi_\lambda | V_{XC}(\lambda) | \psi_\lambda \rangle d\lambda \qquad (2.38)$$

In the λ=0 limit, the electrons are non-interacting and there are consequently no correlation. Since the Kohn-Sham wavefunction is simply a single Slater determinant of orbitals then if the KS orbitals are identical to the HF orbitals, the exact exchange energy is precisely the HF exchange energy:

$$E_X[\phi_i; \lambda = 0] = -\frac{1}{2} \sum_\sigma \sum_{i,j} \int d^3r \int d^3r' \frac{\phi_{i\sigma}^*(r)\phi_{j\sigma}^*(r')\phi_{i\sigma}(r')\phi_{j\sigma}(r)}{|r-r'|} = E_X^{exact} \quad (2.39)$$

The approximation of exchange-correlation can be made by summing E_{XC} terms of different values of λ within the limit λ = 0 to 1. The choice of terms is arbitrary. Hybrid functionals includes a mixture of Hartree-Fock Exchange with DFT exchange-correlation.

B3LYP functional uses Becke's exchange functional with part of the Hartree-Fock exchange mixed in Becke and a scaling factor on the correlation part but using the LYP correlation function.

$$AE_X^{Slater} + (1-A)E_X^{HF} + B\Delta E_X^{Beck} + (1-C)E_C^{VWN} + CE_C^{LYP} \quad (2.40)$$

Where the exchange includes the Slater exchange E_X^{Slater}, or local spin density exchange, along with corrections involving the gradient of the density and the correlation is provided by the LYP and VWN correlations. The constants A, B, and C are those determined by fitting to the G1 molecule set.

2.4. Evaluation of the *threo*:*erythro* product ratio based upon the extended Curtin-Hammett principle.

The thermodynamic properties of ground-state pre-reaction clusters and their corresponding transition structures are used to calculate the *threo*:*erythro* product ratio. The competition between the lowest energy *threo* and *erythro* transition structures constitutes a classic example of the Curtin-Hammett (C-H) principle.[37] The position of the conformational equilibrium can not control the product ratio, since the major product may arise through the reaction of the minor pre-reaction if it has the lowest activation barrier (see Figure 2.1).
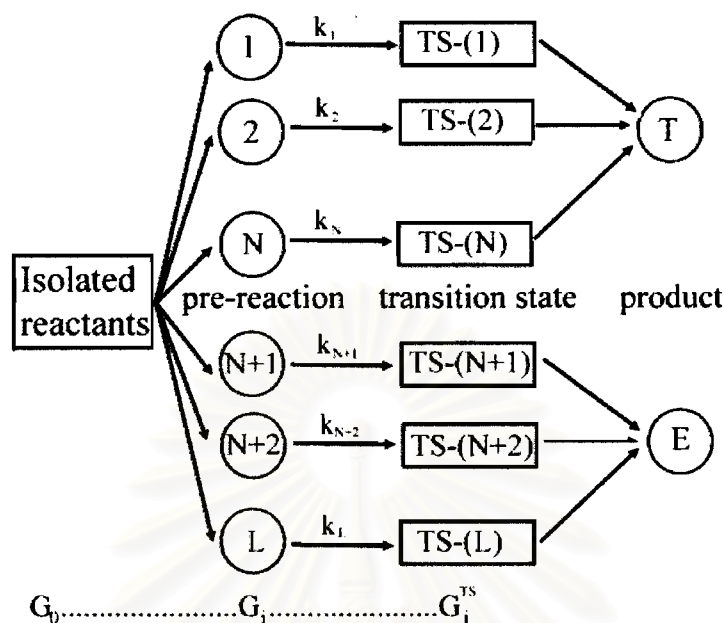
Figure 2.1. Multi-transition state reaction for the formation of the two products *threo* and *erythro*.

For the present multitransition-state system (shown in Figure 3.2) consider the reaction system with $i = 1, 2,.., L$ transition states which can lead to either the T (*threo*) ($i = 1, 2,..., N$) and E (*erythro*) product ($i = N+1, N+2,..., L$). The transition states and reactants have their total free energies denoted by G_i^{TS} and G_i.

According to transition state theory, the rate constant for each individual reaction i is given by Eq 2.41

$$k_i = C.\exp(-\Delta G_i^{\neq} / RT) \tag{2.41}$$

in which $C = æk_BT/h$ (æ is the transmission coefficient, k_B is Boltzmann's constant, h is Planck's constant, T is the absolute temperature) and $\Delta G_i^{\neq} = G_i^{TS} - G_i$.

The ground-state population of each pre-reaction (pi) is determined by the Boltzmann distribution and may be expressed in terms of the free energy differences ($\Delta G_i = G_i - G_0$) with respect to some fixed free energy, G_0 (which may be the free energy of the isolated reactants).Thus, pi is given by Eq 2.42

$$p_i = p_0 . \exp(-\Delta G / RT) \qquad (2.42)$$

Since $\sum\limits_{i=1}^{L} p_i = 1$, it follows from Eq 2.42 that

$$p_i = \exp(-\Delta G / RT) / \sum_{i=1}^{L} \exp(-\Delta G / RT) \qquad (2.43)$$

The product ratio for this multipath reaction may be determined by Eq 2.44, which follows from Eqs 2.41 and 2.43 and holds if the Boltzmann distribution of the pre-reaction clusters is not disturbed during the reaction course.

$$\frac{[T]}{[E]} = \frac{p_1 k_1 + p_2 k_2 + ... + p_N k_N}{p_{N+1} k_{N+1} + p_{N+2} k_{N+2} + ... + p_L k_L} = \frac{\sum\limits_{i=1}^{N} \exp(-(\Delta G_i + \Delta G_i^{\ne}) / RT)}{\sum\limits_{j=N+1}^{L} \exp(-(\Delta G_j + \Delta G_j^{\ne}) / RT)} \qquad (2.44)$$

Substitution of $\Delta G_i = G_i - G_0$ and $\Delta G_i^{\ne} = G_i^{TS} - G_i$ into Eq 2.44 leads to the product ratio based upon the free energies:

$$\frac{[T]}{[E]} = \frac{\sum\limits_{i=1}^{N} \exp(-(\Delta G_i^{TS} - G_0) / RT)}{\sum\limits_{j=N+1}^{L} \exp(-(\Delta G_j^{TS} - G_0) / RT)} = \frac{\sum\limits_{i=1}^{N} \exp(-(\Delta G_i^{TS}) / RT)}{\sum\limits_{j=N+1}^{L} \exp(-(\Delta G_j^{TS}) / RT)} \qquad (2.45)$$

2.5. Method of calculations

All calculations were performed with Gaussian 03 software. Density functional theory as implemented in the restricted B3LYP hybrid exchange correlation scheme was used to include some effects of electron correlation with only a marginal increase in computational cost over Hartree-Fock methods. Density functional theory have been performed with the Becke's three parameters hybrid density functional using the Lee, Yang and Parr correlation functional (B3LYP). All geometry optimizations have been carried out using the hybrid density functional B3LYP at the 6-31G(d). Results have been obtained for geometries optimized in the gas phase. Thermochemistry calculations

have been performed at standard temperature and pressure to account for entropy effects associated with ligand coordination.

The standard enthalpy and Gibbs free energy have been derived from the frequency calculation and entropy were calculated by relation of $\Delta S = (\Delta H - \Delta G)/T$. And the rate constant (k) for an elementary reaction step is defined in terms of the Gibbs activation barrier (ΔG^{*}) as

$$k_i = \kappa \left(\frac{k_B T}{h}\right) \exp\left(\frac{-\Delta G_i^{*}}{RT}\right) = \kappa \left(\frac{k_B T}{h}\right) \exp\left(\frac{\Delta S_i^{*}}{R}\right) \exp\left(\frac{-\Delta H_i^{*}}{RT}\right) \qquad (2.47)$$

Where κ is the transmission coefficient, k_B is the Boltzmann constant, and ΔS_i^{*} and ΔH_i^{*} are the entropic and enthalpic activation barriers, respectively. By incorporating entropy effects, the Gibbs activation barrier provides a more complete representation of intrinsic reaction kinetics at nonzero temperatures than the electronic activation barrier. And for evaluation of the *threo:erythro* product ratio can be given by Eq.2.45.

$$\frac{[Threo]}{[erythro]} = \frac{\sum_{i=1}^{N} \exp(-(\Delta G_i^{*})/RT)}{\sum_{j=N+1}^{L} \exp(-(\Delta G_j^{*})/RT)} \qquad (2.45)$$

When *threo* product has i=1, 2, ..., N transition states and *erythro* product has j= N+1, N+2, ..., L transition states.

CHAPTER III

RESULTS AND DISCUSSION

In this research, mechanisms of epoxidation of three allylic alcohols were investigated. Allylic alcohols 3-methylbut-3-en-2-ol (r1), trans-pent-3-en-2-ol (r2) and cis-pent-3-en-2-ol (r3), used as reactants in epoxidation reactions (are defined as the systems 1, 2 and 3, respectively). Mechanisms of the systems 1, 2 and 3 are generally in the same pattern which is composed of four reaction steps as shown in Figure 3.1. Step 1, the vanadium oxo complex, $VO(OH)_2OOH$ is formed by the oxidation reaction of $VO(OH)_3$ using H_2O_2. The step 1 is a common reaction pathway of all systems. Step 2, the ligand of the vanadium oxo complex is substituted by allylic alcohol to form VO(OH)(OOH)OCHMeCR=CR'R" as intermediate int2rt (or int2re). Step 3 is the oxygen transfer of the intermediate int2rt (or int2re) to form intermediate int3rt (or int3re). Step 4, the epoxidized product int4rt (or int4re) is finally formed.

The transition state of the step 2 is critical for whether *threo* or *erythro* diastereoselectivity. The *threo* and *erythro* conformations are defined as an exo and an endo attack site conformation, respectively. The exo and endo sites possess the dihedral angle O1V2LxLy within 0-90 and 90-180 degrees, respectively. Atomic numbering and the attack sites are shown in Figures 3.2 and 3.3, respectively.

The geometrical data for transition-state structures (ts1a and ts1b) of step 1, listed in Table 3.1 show that ts1a and ts1b are the exo and endo conformations, respectively. The energies and thermodynamic properties of activation for the formation of vanadium hydrogenperoxo complex are listed in Table 3.2. This step, the attacking position is shown by dihedral angle O1V2O3O4. The ts1a and ts1b have dihedral angle O1V2O3O4 to be 40.8 and 168.0 degree, respectively. For the transition state, hydrogen peroxide transfers hydrogen from the oxygen coordinating the vanadium center to nearest hydroxyl group. This proton-transfer step in the transformation of the coordinated hydrogen peroxide ligand into a hydroperoxo group on vanadium favor the exo site, because less steric. The activation energy of exo site (ts1b, 5.54 kcal/mol) is lower than the endo site (ts1a, 8.83 kcal/mol). The geometrical

structures of transition-state of the vanadium hydrogenperoxo complex are shown in Figure 3.4.

The geometrical data for all transition-state structures (systems 1, 2 and 3) of step 2 are tabulated in Table 3.3. The attacking position is shown by dihedral angle O1V2O6C8. Due to the dihedral angle O1V2O6C8, these transition structures are the categorized into *threo-* and *erythro-* conformations. Energies, thermodynamic properties, kinetic constants of activation and reaction constants of epoxidation of systems 1, 2 and 3 of step 2 are listed in Table 3.4. Table 3.4 shows that the activation energies due to *threo*-transition states of system 1 are lower than *erythro*-transition states, but in systems 2 and 3, *erythro*-transition states are lower than *threo*-transition states. Log K of *threo*-transition states are lower than *erythro*-transition states. These thermodynamic properties show the competition of selectivity. This step, the transition structures of the system 1, 2 and 3 are show in Figure 3.5.

Geometrical data for transition structures of systems 1, 2 and 3, (step 3) are listed in Table 3.5 and shown in Figure 3.6. The ideal *spiro* TSs possessed the interplanar angle, φ between V2O3O4 plane and O4C8C9 plane, 90°, while for the *planar* geometry it is 0°; determination of interplanar angle φ is described in Appendix A. This result has a more pronounced *spiro* transition character (φ of plane is about 71.8-89.9°, Table 3.5) and have dihedral angle O6C7C8C9 is about 32.2-52.5. This step, *threo*-pathway is preference than *erythro*-pathway (considered by $E^{\neq}$ in Table 3.6). Energies and thermodynamic properties of activation and reaction of the oxygen-transfer are listed in Tables 3.6. The activation enthalpies ($\Delta H^{\neq}$) for oxygen transfer have range between 13.58 and 16.60 kcal/mol (shown in Table 3.6). This result is in the range of the available experimental data for metal catalyzed epoxidations, since it was reported that the activation enthalpies for vanadium catalyzed *tert*-butyl hydroperoxide epoxidation of cyclohexene is 12.7 kcal/mol and molybdenum catalyzed *tert*-butyl hydroperoxide epoxidation of octane is 18 kcal/mol.[37]

For the last step (step 4), the geometrical data for all transition structures of systems 1, 2 and 3 are listed in Table 3.7 and shown in Figure 3.7. The attacking position is shown by dihedral angle O1V2O4C5. One system has eight pathways to substite the ligand. For system 1, the rate constants for *erythro*-pathways indicated by log k are smaller than rate constants for the *threo*-pathways (Table 3.8). But sytems 2

and 3, the rate constants for *erythro*-pathways indicated by log k are larger than rate constants for the *threo*-pathways. Energies and thermodynamic properties of activation and reaction of this step are listed in Tables 3.8.

The energy profiles of the epoxidation reaction of the systems 1, 2 and 3 are shown in Figures 3.8, 3.9 and 3.10, respectively.

Evaluation of the *threo*:*erythro* product ratio.

As the step 2 is the determining step for computing the *threo*:*erythro* product ratio, the kinetic constants (k) of this activation step for each system were therefore used to compute the product ratio using the Curtin-Hammett method. This method have been used to estimate the *threo*:*erythro* product ratio of the diastereoselective for titanium catalyzed *tert*-butyl hydroperoxide epoxidation. Those computational results are in good agreement with the experimental diastereoselectivity.[37] The calculated *threo*:*erythro* ratios are 12:88 (r1) and 92:8 (r2), which are in good accordance with the experimental values 22:78 (r1) and 91:9 (r2).

For the diastereoselective for vanadium catalyzed hydroperoxide epoxidation, the *threo*:*erythro* ratios of substrates r1, r2 and r3 (corresponding to the systems 1, 2 and 3, respectively) computed using the Curtin-Hammett principle are 99.7:0.3, 80.9:19.1 and 72.2:27.8, respectively (Table 3.9.).
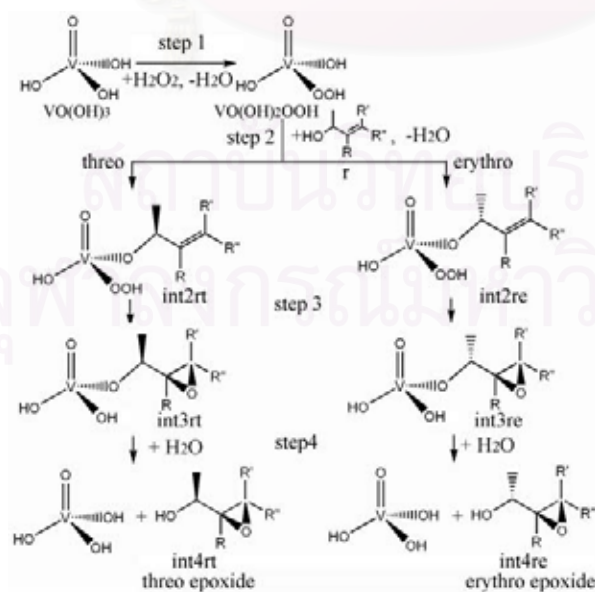
Figure 3.1. Pathway of diastereoselective epoxidation of allylic alcohol by vanadium peroxy complex.
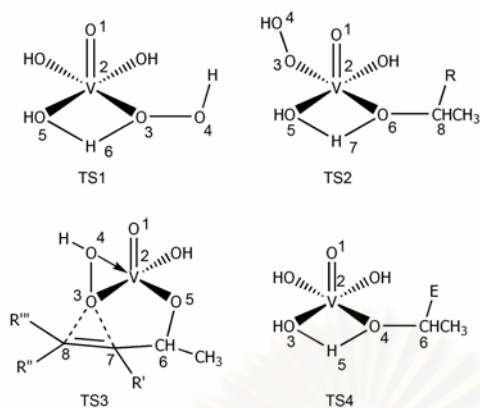
Figure 3.2. The labeling atom of transition state in epoxidation by vanadium peroxy complex.
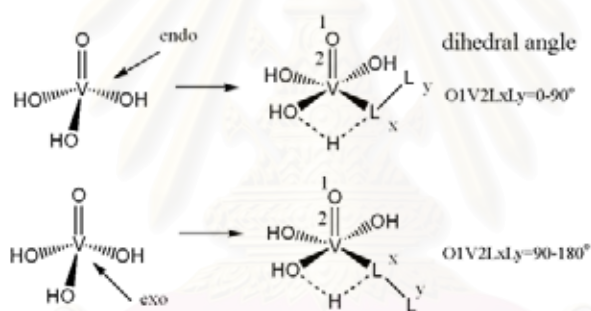
Figure 3.3. The attack site of ligand on vanadium complex.

Table 3.1. Geometrical data for transition structures of the formation of vanadium hydrogenperoxo complex (step 1), optimized at B3LYP/6-31G(d) level of theory

Transition structure	Dihedral[a]		Bond length[b]			
	O1V2O3O4	O1V2O5H6	V2O3	V2O5	O3H6	O5H6
ts1a	40.8	61.3	2.145	2.000	1.222	1.190
ts1b	168.0	110.2	2.117	2.027	1.250	1.178

[a] In degree. [b] In angstrom.

ts1a
endo site

ts1b
exo site
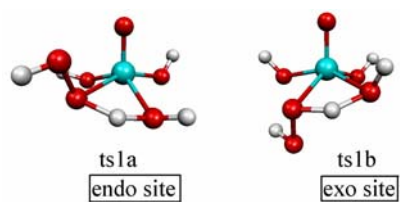
Figure 3.4. The B3LYP/6-31G(d)-optimized structures of transition state in the formation

of vanadium   hydrogenperoxo complex (step 1).

Table 3.2. Energies and thermodynamic properties of activation for the formation of

vanadium   hydrogenperoxo complex (step 1), computed at B3LYP/6-

31G(d) level of theory

	Transition state					reaction				
	$E^{\ddagger,a}$	$\Delta H^{\ddagger,a}$	$\Delta G^{\ddagger,a}$	$\Delta S^{\ddagger,b}$	Log k	ΔE^a	ΔH^a	ΔG^a	ΔS^b	Log K
$VO(OH)_3$-ts1a-$VO(OH)_2OOH$	8.83	9.35	19.63	-34.48	-1.60	-1.93	-0.56	-1.21	-0.47	0.89
$VO(OH)_3$-ts1b-$VO(OH)_2OOH$	5.54	5.47	16.23	-36.09	0.89					

^{a} In kcal mol^{-1}. ^{b} In cal mol^{-1}K^{-1}.

Table 3.3. Geometrical data for transition structures of substitution of substrate on vanadium hydrogenperoxo complex (step 2), optimized at B3LYP/6-31G(d) level of theory

parameter	Dihedral[a]			Bond length[b]						
	O1V2O3O4	O1V2O6C8	O1V2O5H7	V2O3	O3O4	V2O4	V2O5	V2O6	O5H7	O6H7
System 1										
ts2r1ta	177.4	47.2	103.0	1.813	1.456	2.302	2.040	2.022	1.178	1.246
ts2r1tb	167.9	102.9	93.4	1.808	1.454	2.286	2.135	2.016	1.179	1.238
ts2r1ea	72.2	15.8	84.7	1.846	1.445	2.133	2.031	2.043	1.196	1.225
ts2r1eb	67.7	128.3	81.1	1.840	1.446	2.250	2.046	2.064	1.185	1.224
System 2										
ts2r2ta	176.9	49.6	103.6	1.813	1.456	2.305	2.041	2.015	1.177	1.249
ts2r2tb	64.6	129.3	89.2	1.845	1.450	2.304	2.050	2.008	1.188	1.225
ts2r2ea	72.0	16.4	84.7	1.846	1.445	2.137	2.034	2.034	1.195	1.228
ts2r2eb	68.6	135.5	82.5	1.840	1.446	2.239	2.051	2.061	1.181	1.231
System 3										
ts2r3ta	177.2	49.0	103.9	1.813	1.456	2.304	2.041	2.015	1.177	1.249
ts2r3tb	64.6	128.4	89.1	1.845	1.450	2.302	2.050	2.008	1.189	1.223
ts2r3ea	72.0	16.8	84.5	1.846	1.445	2.137	2.033	2.033	1.196	1.226
ts2r3eb	64.8	131.2	89.9	1.844	1.451	2.299	2.052	2.006	1.197	1.214

[a] In degree.   [b] In angstrom.
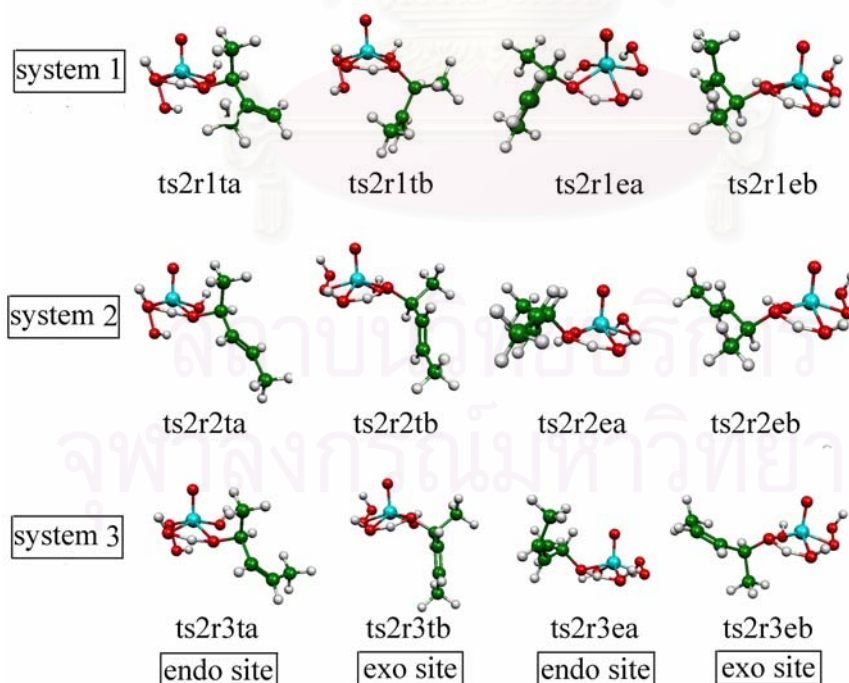
Figure 3.5. The B3LYP/6-31G(d)-optimized structures of transition state in the substitution of substrate on vanadium hydrogenperoxo complex (step 2).

Table 3.4. Energies and thermodynamic properties for the substitution of substrate on vanadium hydrogenperoxo complex (step 2), computed at B3LYP/6-31G(d) level of theory

	Transition state					reaction				
	$E^{\ddagger,a}$	$\Delta H^{\ddagger,a}$	$\Delta G^{\ddagger,a}$	$\Delta S^{\ddagger,b}$	Log k	$\Delta E^{,a}$	$\Delta H^{,a}$	$\Delta G^{,a}$	$\Delta S^{,b}$	Log K
System 1										
VO(OH)$_2$OOH-ts2r2ta-int2r2t	6.03	5.88	17.64	-39.46	-0.14	1.01	2.87	2.48	1.27	-1.82
VO(OH)$_2$OOH-ts2r2tb-int2r2t	2.65	2.30	14.94	-42.42	1.84					
VO(OH)$_2$OOH-ts2r1ea-int2r1e	6.13	5.62	18.68	-43.80	-0.90	-0.89	0.37	0.69	-1.06	-0.51
VO(OH)$_2$OOH-ts2r1eb-int2r1e	6.33	5.86	19.06	-44.27	-1.18					
System 2										
VO(OH)$_2$OOH-ts2r2ta-int2r2t	6.15	5.98	17.76	-39.53	-0.23	1.04	2.90	1.99	3.04	-1.46
VO(OH)$_2$OOH-ts2r2tb-int2r2t	7.50	7.30	19.47	-40.80	-1.48					
VO(OH)$_2$OOH-ts2r2ea-int2r2e	6.10	5.53	18.69	-44.13	-0.91	-0.89	0.37	0.69	-1.36	-0.51
VO(OH)$_2$OOH-ts2r2eb-int2r2e	6.92	6.41	19.68	-44.51	-1.64					
System 3										
VO(OH)$_2$OOH-ts2r3ta-int2r3t	5.55	5.24	17.48	-41.06	-0.02	0.42	2.13	2.41	-0.94	-1.77
VO(OH)$_2$OOH-ts2r3tb-int2r3t	6.84	6.55	18.99	-41.74	-1.13					
VO(OH)$_2$OOH-ts2r3ea-int2r3e	5.48	5.42	18.11	-42.56	-0.48	0.08	1.26	1.48	-0.76	-1.09
VO(OH)$_2$OOH-ts2r3eb-int2r3e	7.29	7.64	19.10	-38.42	-1.21					

[a] In kcal mol^{-1}.   [b] In cal mol^{-1}K^{-1}.

Table 3.5. Geometrical data for transition structures of the oxygen-transfer reaction

(step 3), optimized at B3LYP/6-31G(d) level of theory

Transition structure	Dihedral[a] O6C7C8C9	Interplanar angle[a]	Bond length [,b]					
			V2O3	V2O4	O3O4	O3C8	O3C9	C8C9
System 1								
ts3r1t	32.2	76.2	1.909	1.980	1.757	2.220	2.122	1.361
ts3r1e	33.6	86.4	1.984	1.905	1.749	2.243	2.123	1.362
System 2								
ts3r2t	34.0	76.8	1.912	1.979	1.756	2.161	2.181	1.361
ts3r2e	38.2	89.2	1.980	1.909	1.753	2.167	2.177	1.360
System3								
ts3r3t	44.8	72.8	1.974	1.918	1.759	2.153	2.313	1.365
ts3r3t	52.5	71.8	1.975	1.914	1.759	2.134	2.198	1.364

[a] In degree.   [b] In angstrom.
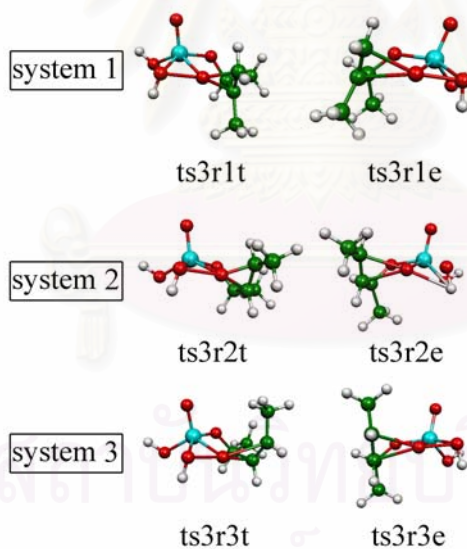
Figure 3.6. The B3LYP/6-31G(d)-optimized structures of transition state in the oxygen-transfer reaction (step 3).

Table 3.6. Energies and thermodynamic properties for the oxygen-transfer reaction (step 3), computed at B3LYP/6-31G(d) level of theory

	Transition state					reaction				
	$E^{\ddagger,a}$	$\Delta H^{\ddagger,a}$	$\Delta G^{\ddagger,a}$	$\Delta S^{\ddagger,b}$	Log k	$\Delta E^{,a}$	$\Delta H^{,a}$	$\Delta G^{,a}$	$\Delta S^{,b}$	Log K
System 1										
int2r1t-ts3r1t-int3r1t	14.85	14.11	17.24	-12.60	-0.31	-47.38	-47.86	-46.02	-6.16	33.74
int2r1e-ts3r1e-int3r1e	16.6	16.28	19.03	-9.22	-1.15	-50.73	-50.65	-49.16	-5.00	36.04
System 2										
int2r2t-ts3r2t-int3r2t	12.91	11.44	15.97	-15.19	1.09	-51.81	-52.99	-49.67	-11.16	36.41
int2r2e-ts3r2e-int3r2e	15.04	14.78	17.42	-8.86	0.02	-48.46	-48.39	-47.11	-4.28	34.54
System 3										
int2r3t-ts3r3t-int3r3t	13.58	12.77	16.01	-10.86	1.05	-50.48	-51.46	-49.8	-5.56	36.51
int2r3e-ts3r3e-int3r3e	13.61	13.32	16.52	-10.73	0.69	-51.18	-51.72	-49.05	-8.95	35.96

[a] In kcal mol^{-1}.   [b] In cal mol^{-1}K^{-1}.

Table 3.7. Geometrical data for transition structures of the substitution of water to convert catalyst and epoxide product (step 4), optimized at B3LYP/6-31G(d) level of theory

Transition structure	Dihedral[a]		Bond length[b]			
	O2V2O4C6	O2V2O3H5	V2O3	V2O4	O3H5	O4H5
System 1						
ts4r1ta	35.0	88.1	2.052	2.006	1.186	1.243
ts4r1tb	122.9	88.1	2.051	2.047	1.190	1.227
ts4r1tc	74.5	77.2	2.070	2.044	1.197	1.216
ts4r1td	124.7	82.5	2.041	2.123	1.164	1.248
ts4r1ea	58.2	93.6	2.030	2.004	1.280	1.146
ts4r1eb	145.2	113.8	2.078	2.030	1.271	1.154
ts4r1ec	3.5	72.9	2.039	2.062	1.214	1.216
ts4r1ed	146.2	114.3	2.072	2.037	1.267	1.158
System 2						
ts4r2ta	58.2	93.8	2.017	1.964	1.201	1.180
ts4r2tb	122.0	88.3	2.051	2.045	1.191	1.226
ts4r2tc	5.7	76.5	2.067	2.046	1.191	1.226
ts4r2td	126.0	82.0	2.043	2.120	1.163	1.250
ts4r2ea	17.7	76.6	2.048	2.096	1.202	1.226
ts4r2eb	150.2	112.9	2.075	2.037	1.268	1.159
ts4r2ec	5.5	77.0	2.071	2.045	1.1 94	1.222
ts4r2ed	146.5	114.4	2.071	2.038	1.268	1.158
System 3						
ts4r3ta	40.4	88.9	2.048	2.007	1.247	1.1 78
ts4r3tb	122.4	88.4	2.050	2.043	1.193	1.124
ts4r3tc	22.8	72.6	2.051	2.086	1.241	1.286
ts4r3td	127.3	83.4	2.044	2.118	1.163	1.250
ts4r3ea	2.1	74.9	2.070	2.041	1.208	1.209
ts4r3eb	149.6	114.2	2.072	2.034	1.270	1.157
ts4r3ec	4.7	76.7	2.072	2.043	1.196	1.221
ts4r3ed	144.7	115.0	2.069	2.035	1.270	1.157

[a] In degree.   [b] In angstrom.

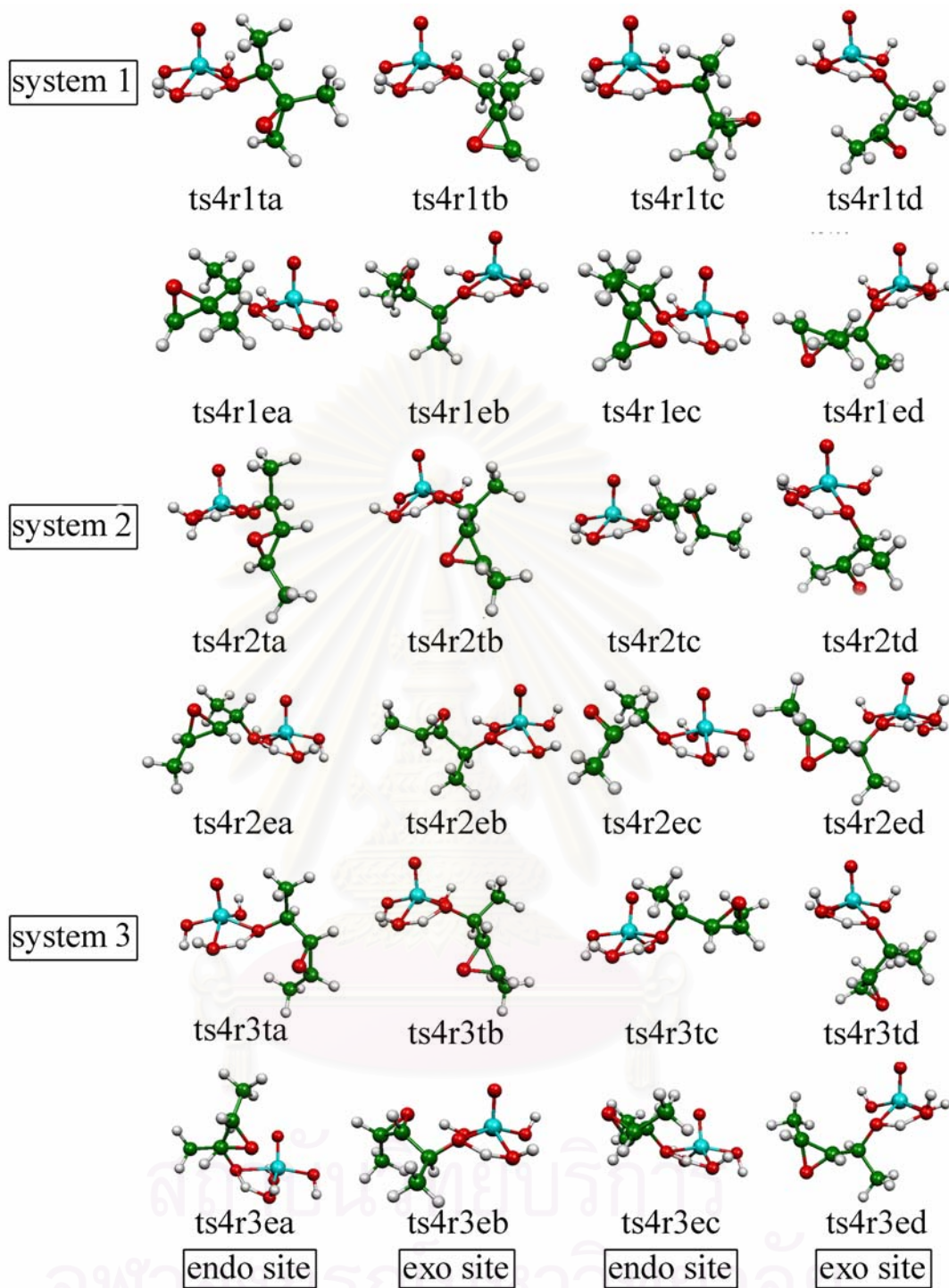**Figure 3.7.** The B3LYP/6-31G(d)-optimized structures of transition state in the substitution of water to convert catalyst and epoxide product (step 4).

Table 3.8. Energies and thermodynamic properties for the substitution of water to convert catalyst and epoxide product (step 4), computed at B3LYP/6-31G(d) level of theory

	Transition state					reaction				
	$E^{\ddagger,a}$	$\Delta H^{\ddagger,a}$	$\Delta G^{\ddagger,a}$	$\Delta S^{\ddagger,b}$	Log k	$\Delta E^{,a}$	$\Delta H^{,a}$	$\Delta G^{,a}$	$\Delta S^{,b}$	Log K
System 1										
int3r1t-ts4r1ta-int4r1t	8.88	7.00	17.96	-36.75	-0.37	-2.20	-3.98	-4.37	1.28	3.20
int3r1t-ts4r1tb-int4r1t	7.96	6.06	17.71	-39.08	-0.19					
int3r1t-ts4r1tc-int4r1t	9.8	8.02	18.68	-35.76	-0.9					
int3r1t-ts4r1td-int4r1t	3.42	1.13	23.96	-43.02	2.56					
int3r1e-ts4r1ea-int4r1e	18.17	16.12	27.64	-38.65	-7.47	2.23	0.40	-0.39	2.64	0.28
int3r1e-ts4r1eb-int4r1e	12.43	10.54	22.12	-38.82	-3.42					
int3r1e-ts4r1ec-int4r1e	12.08	10.78	21.54	-36.11	-3.00					
int3r1e-ts4r1ed-int4r1e	13.00	11.23	21.85	-35.63	-3.22					
System 2										
int3r2t-ts4r2ta-int4r2t	22.01	18.06	34.46	-55.00	-3.64	3.81	2.79	1.76	3.47	-1.29
int3r2t-ts4r2tb-int4r2t	11.81	10.58	21.12	-35.37	-1.99					
int3r2t-ts4r2tc-int4r2t	14.16	13.52	23.23	-32.56	-2.04					
int3r2t-ts4r2td-int4r2t	12.65	12.06	21.58	-31.94	0.07					
int3r2e-ts4r2ea-int4r2e	5.69	3.32	16.41	-43.92	-2.75	3.5	2.54	0.62	6.44	-0.46
int3r2e-ts4r2eb-int4r2e	8.77	6.9	18.61	-39.30	-1.88					
int3r2e-ts4r2ec-int4r2e	10.77	9.58	19.75	-34.13	-2.20					
int3r2e-ts4r2ed-int4r2e	9.88	8.09	18.86	-36.14	-1.73					
System 3										
int3r3t-ts4r3ta-int4r3t	12.62	11.27	22.41	-37.37	-3.64	3.81	2.80	1.76	3.47	-1.29
int3r3t-ts4r3tb-int4r3t	10.22	8.89	20.17	-37.84	-1.99					
int3r3t-ts4r3tc-int4r3t	9.28	8.23	20.24	-40.29	-2.04					
int3r3t-ts4r3td-int4r3t	6.27	4.50	17.35	-43.11	0.07					
int3r3e-ts4r3ea-int4r3e	12.32	11.62	21.21	-32.15	-2.75	3.50	2.54	0.62	6.44	-0.46
int3r3e-ts4r3eb-int4r3e	10.76	9.40	20.01	-35.58	-1.88					
int3r3e-ts4r3ec-int4r3e	11.95	10.76	20.45	-32.47	-2.20					
int3r3e-ts4r3ed-int4r3e	11.05	10.42	19.81	-31.51	-1.73					

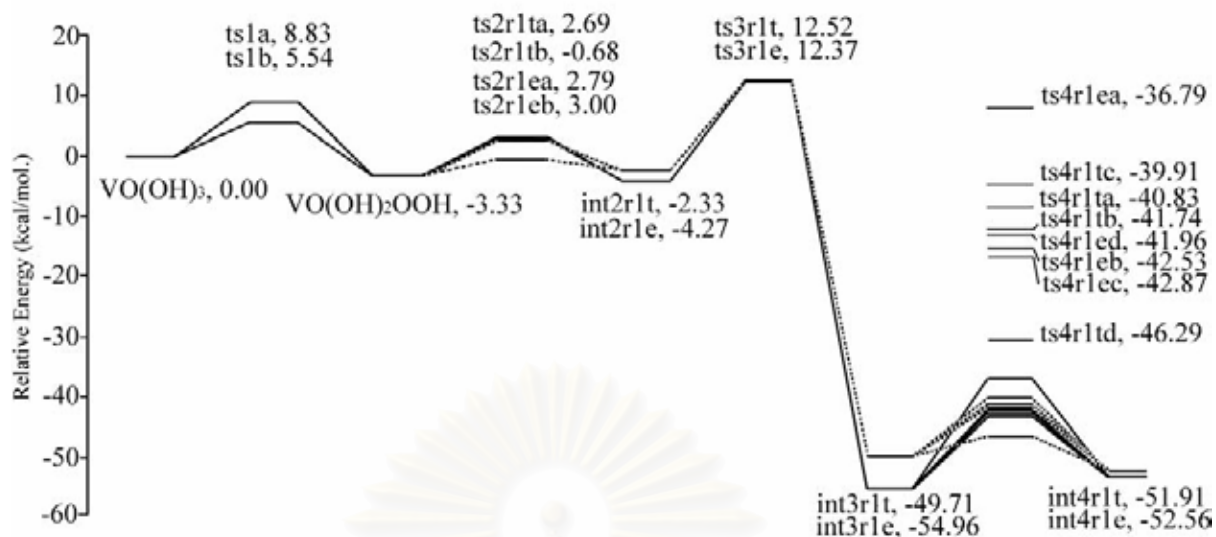[a] In kcal mol^{-1}.   [b] In cal mol^{-1}K^{-1}.

Figure 3.8. Energy profile of the epoxidation reaction of system 1 (3-methylbut-3-en-2-ol, r1).
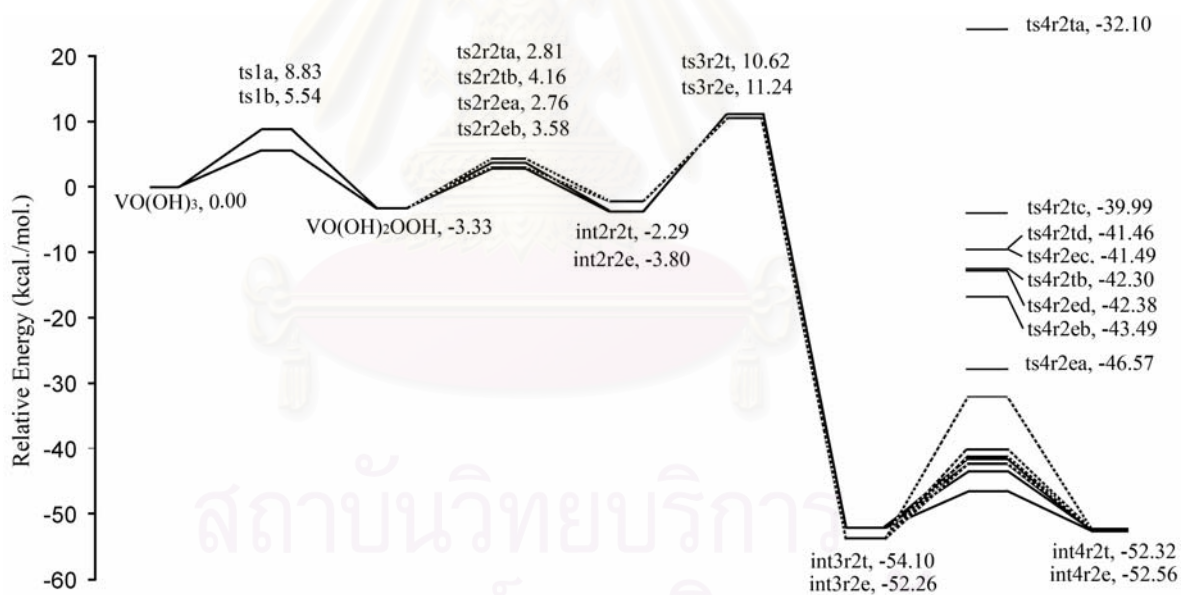

Figure 3.9. Energy profile of the epoxidation reaction of system 2 (trans-pent-3-en-2-ol, r2).
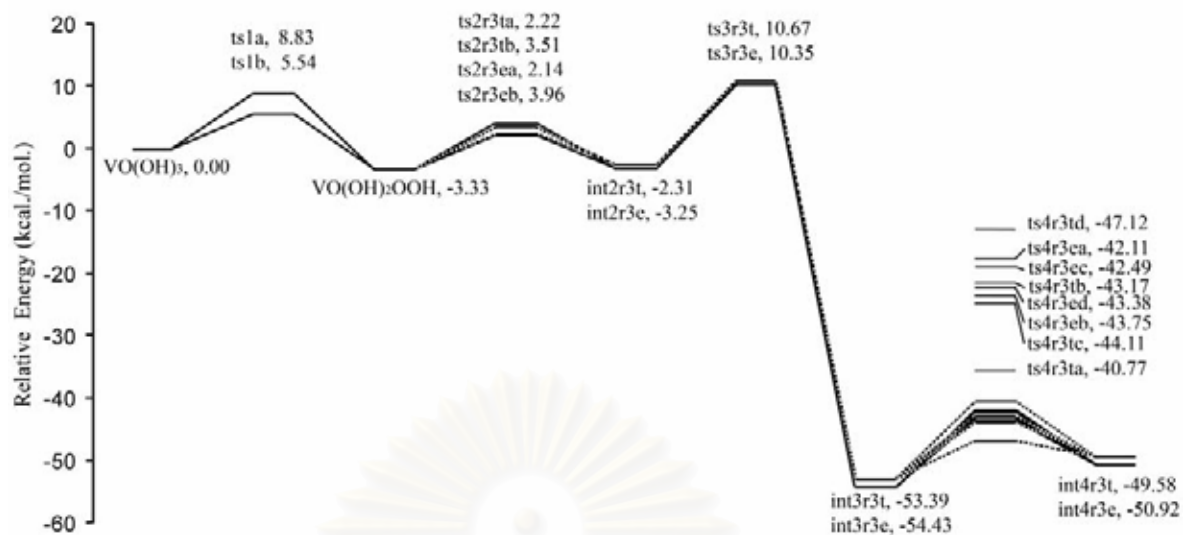
Figure 3.10. Energy profile of the epoxidation reaction of system 3 (cis-pent-3-en-2-ol, r3).

Table 3.9. The *threo*:*erythro* ratio for the epoxidation of systems 1, 2 and 3 computed using the Curtin-Hammett principle

system	subsrtrate	*threo*:*erythro* ratio
1	r1	99.7:0.03
2	r2	80.9:19.1
3	r3	72.2:27.8

CHAPTER IV

CONCLUSIONS AND SUGGESTIONS

The structures of all reactants, intermediates, transition states and products are optimized using the densitity functional theory method at B3LYP/6-31G(d) level of theory. The four reactions steps were found. The first is the common reaction pathway and the second step is the pathway to form intermediate of allylicalcohol-substitution vanadium oxo complex. The third step is the oxygen-transfer process and final step is the ligand-substitution to give product and release catalysts. The results of calculation can be concluded as follows:

1. The exo and endo attack-site give the *threo-* and *erythro-* conformer products via the second step.

2. The *threo*:*erythro* product ratio of each system of reactant depends upon the kinetic rate due to the second step.

3. The *threo*:*erythro* product ratios for systems 1, 2 and 3 are approximately 99.7:0.3, 80.9:19.1 and 72.2:27.8, respectively.

Sugesstion for further work:

The solvation effect of ligand in the transition-metal complex and electronic properties of their structures should be studied. The structure-activation-relationship can be performed to design new and more potent catalysts.

As the results according to Curtin-Hammett method are in good agreement with the experimetal diastereoselectivity in epoxidation, it may be applied to evaluate the selectivity of the other reaction, such as the propylene glycol dehydration.

REFERENCES

1. Denmark, S. E.; Matsuhashi, H. "Chiral Fluoro Ketones for Catalytic Asymmtric Epoxidation of Alkenes with Oxone" *J. Org. Chem.*, **2002**, *67*, 3479-3486.

2. Yun, D. W.; David K. W. L. "A Density Functional Study on the Stereocontrol of the Sharpless Epoxidation" *J. Am. Chem. Soc.,* **1995,** *117***,** 11327-11336.

3. Alice, E. L.; Aaron, M.; Ann, R. K.; Patrick, J. C. Patrick, J. W. "Highly Enantio-and Diastereoselective One-Pot Synthesis of Acyclic Epoxy Alcohols with Three Contiguous Stereocenters" *J. Am. Chem. Soc.,* **2004**, *126*, 13608-13609.

4. Rudolph, J.; Reddy, K. L.; Chiang, J. P.; Sharpless, K. B. "Highly Efficient Epoxidation of Olefins Using Aqueous H2O2 and Catalytic Methyltrioxorhenium/ Pyridine: Pyridine-Mediated Ligand Acceleration" *J. Am. Chem. Soc.,* **1997,** *119,* 6189-6190.

5. Murase, N.; Hoshino, Y.; Oishi, M. Yamamoto, H.; "Chiral Vanadium-Based Catalysts for Asymmetric Epoxidation of Allylic Alcohols" *J. Org. Chem.,* **1999,** *64,* 338-339.

6. Lempers, H. E. B.; Garcia, A. R.; Sheldon, R. A.; "Metal-Catalyzed Oxidations with Pinane Hydroperoxide: A Mechanistic Probe To Distinguish between Oxometal and Peroxometal Pathways" *J. Org. Chem.,* **1998**, *63,* 1408-1413.

7. Palucki, M.; Finney, N. S.; Pospisil, P. J. Guler, M. L.; Ishida, T.; Jacobsen, E. N.; "The Mechanistic Basis for Electronic Effects on Enantioselectivity in the (salen) Mn(III)-Catalyzed Epoxidation Reaction" *J. Am. Chem. Soc.,* **1998**, *120,* 948-954.

8. Ready, J. M.; Jacobsen, E. N. "Highly Active Oligomeric (salen)Co Catalysts for Asymmetric Epoxide Ring-Opening Reactions" *J. Am. Chem. Soc.,* **2001,** *123,* 2687-2688.

9. Chang, S.; Lee, H. L.; Jacobsen, E. N. "Regio- and Enantioselective Catalytic Epoxidation of Conjugated Polyenes. Formal Synthesis of LTAd Methyl Ester" *J.Org. Chem.,* **1993**, *58***,** 25, 6939-6941.

10. Brandes, B. D.; Jacobsen, E.N. "Highly Enantioselective, Catalytic Epoxidation of Trisubstituted Olefins" *J. Org. Chem.,* **1994,** *59*, 4378-4380.

11. Houk, K. N.: Liu, J.; DeMello, N. C.; Condroski K. R. **"**Transition States of epoxidations: Diradical Character, Spiro Geometries, Transition State Flexibility, and the Origins of Stereoselectivity" *J. Am. Chem. Soc.,* **1997,** *119,*10147-10152.

12. Liu, J.;Houk,K. N. "Dioxirane Epoxidations of 1,1-Disubstituted Ethylenes Probing for Radical Pathways by Computations and Experiments" *J. Org. Chem.,* **1998**, *63,* 8565-8569.

13. Anderson, D. R.; Woods, K. W.; Beak, P. "The Endocyclic Restriction Test: Oxygen Transfer from *N*-Sulfonyl Oxaziridines to Alkenes" *Org. Lett.,* **1999**, 1, 9, 1415-1417.

14. Bach, R. D.; Glukhovtsev, M. N.; Gonzalez, C. "High-Level Computational Study of the Stereoelectronic Effects of Substituents on Alkene Epoxidations with Peroxyformic Acid" *J. Am. Chem. Soc.,* **1998**, *120,* 9902-9910.

15. Sinclair, P.E.; Catlow, C. R. A. "Quantum Chemical Study of the Mechanism of Partial Oxidation Reactivity in Titanosilicate Catalysts: Active Site Formation, Oxygen Transfer, and Catalyst Deactivation" *J. Phys. Chem. B,* **1999**, *103,* 1084-1095.

16. Cui, M.; Adam, W.; Shen, J. H.; Luo, X. M.; Tan, X. J.; Chen, K. X.; Ji, R. Y.; Jiang, H. L. "A Density-Functional Study of the Mechanism for the Diastereoselective Epoxidation of Chiral Allylic Alcohols by the Titanium Peroxy Complexes" *J. Org. Chem.,* **2002**, *67,* 1427-1435.

17. Munakata, H.; Oumi, Y.; Miyamoto, A. "A DFT Study on Peroxo-Complex in Titano-silicate Catalyst: Hydrogen Peroxide Activation on Titanosilicalite-1 Catalyst and Reaction Mechanisms for Catalytic Olefin Epoxidation and for Hydroxyl-amine Formation from Ammonia" *J. Phys. Chem. B,* **2001**, *105,* 3493-3501.

18. Adam, W.; Alsters, P. L.; Neumann, R.; Saha-Moller, C. R.; Seebach, D.; Beck, A. K.; Zhang, R. "Chiral Hydroperoxides as Oxygen Source in the Catalytic Stereoselective Epoxidation of Allylic Alcohols by Sandwich-Type Polyoxometalates: Control of Enantioselectivity through a Metal-Coordinated Template" *J. Org. Chem.,* 2003, *68,* 8222-8231.

19. Valentin, C. D.; Gisdakis, P.; Yudanov, I. V.; Rosch, N. "Olefin Epoxidation by Peroxo Complexes of Cr, Mo, and W. A Comparative Density Functional Study"*J. Org. Chem.,* **2000**, *65,* 2996-3004.

20. Lane, B. S.; Burgess, K. "Metal-Catalyzed Epoxidations of Alkenes with Hydrogen Peroxide" *Chem. Rev*, **2003**, *103*, 7, 2457-2473.

21. Morgan, K. M.; Gronert, S. "Structural and Solvent Effects on the Mechanism of Base-Induced Rearrangement of Epoxides to Allylic Alcohols" *J. Org. Chem.,* **2000**, *65,* 1461-1466.

22. Yao, H.; Richardson, D. E. "Epoxidation of Alkenes with Bicarbonate-Activated Hydrogen Peroxide" *J. Am. Chem. Soc.,* **2000**, *122,* 3220-3221.

23. Adam, W.; Smerz, A. K. "Solvent Effects in the Regio- and Diastereoselective Epoxidations of Acyclic Allylic Alcohols by Dimethyldioxirane: Hydrogen Bonding as Evidence for a Dipolar Transition State" *J. Org. Chem.,* **1996**, *61,* 3506-3510.

24. Chong, A. O.; Sharpless, K. B. "On the Mechanism of the Molybdenum and Vanadium Catalyzed Epoxidation of Olefins by Alkyl Hydroperoxides" *J. Org. Chem.,* **1977**, *42, 9,* 1987-1990.

25. Bolm, C. "Vanadium-catalyzed asymmetric oxidations" *Coord. Chem. Rev.,* **2003**, *237*, 245-256.

26. Mimom, H.; Mignard, M.: Brechot, P.; Saussine, L. "Selective Epoxidation of Olefins by Oxo[*N-(2-oxidophenyl)salicylidenaminato*]vanadium(V) Alkyl peroxides: On the Mechanism of the Halcon Epoxidation Process" *J. Am. Chem. Soc.*, **1986**, *108*, 3711-3718.

27. Lubben, T. V.; Wolczanski, P. T. "Dioxygen Activation by Group 4 tritox Alkyls (tritox =t-Bu3CO-): Insertion and Oxygen Atom Transfer" *J. Am. Chem. Soc.,* **1987**, *109,* 424-435.

28. Michaelson, R. C.; Palermo, R. E.; Sharpless, K. B. "Chiral Hydroxamic Acids as Ligands in the Vanadium Catalyzed Asymmetric Epoxidation of Allylic Alcoholsby *tert*-Butyl Hydroperoxide" *J. Am. Chem. Soc.,* **1977***,* 1990-1992.

29. Itoh, T.; Jitsukawa, K.; Kaneda, K.; Teranishi, S. "Vanadium-Catalyzed Epoxidation of Cyclic Allylic Alcohols. Stereoselectivity and Stereocontrol Mechanism" *J. Am. Chem. Soc.,* **1979***, 101,* 1990-1992.

30. Hoshino, Y.; Yamamoto, H. "Novel α-Amino Acid-Based Hydroxamic Acid Ligands for Vanadium-Catalyzed Asymmetric Epoxidation of Allylic Alcohols" *J. Am. Chem, Soc.,* **2000**, *122,* 10452-10453.

31. Adam, W.; Mitchell, C. M.; R. SahaMoller, C. R. "Regio- and Diastereoselective Catalytic Epoxidation of Acyclic Allylic Alcohols with Methyltrioxorhenium: A Mechanistic Comparison with Metal (Peroxy and Peroxo Complexes) and Nonmetal (Peracids and Dioxirane) Oxidants" *J. Org. Chem.,* **1999**, *64,* 3699- 3707.

32. Freccero, M.; Gandolfi, R.; Sarzi-Amade, M.; Rastelli, A. "Facial Selectivity in Epoxidation of 2-Cyclohexen-1-ol with Peroxy Acids. A Computational DFT Study" *J. Org. Chem.,* **2000**, *65,* 8948-8959.

33. Freccero, M.; Gandolfi, R.; Sarzi-Amade, M.; Rastelli, A. "Epoxidation of Acyclic Chiral Allylic Alcohols with Peroxy Acids: Spiro or Planar Butterfly Transition Structures A Computational DFT Answer" *J. Org. Chem.,* **2000**, *65,* 2030-2042.

34. Bach, R. D.; Canepa, C.; Winter, J. E.; Blanchette, P. E. "Mechanism of Acid-Catalyzed Epoxidation of Alkenes with Peroxy Acids" *J. Org. Chem.,* **1997**, *62,* 5191-5197.

35. Houk, K. N.; Liu, J.; DeMello, N. C.; Condroski, K. R. "Transition States of Epoxidations: Diradical Character, Spiro Geometries, Transition State Flexibility, and the Origins of Stereoselectivity" *J. Am. Chem. Soc.,* **1997,** *119*, 10147-10152.

36. Adam, W.; Mitchell, C. M.; Saha-Moller, C. R. "Regio- and Diastereoselective Catalytic Epoxidation of Acyclic Allylic Alcohols with Methyltrioxorhenium: A Mechanistic Comparison with Metal (Peroxy and Peroxo Complexes) and Nonmetal (Peracids and Dioxirane) Oxidants" *J. Org. Chem.,* **1999**, *64,* 3699- 3707.

37. Adam, W.;Bach, R.D.; Dmitrenko, O.; Chantu, R. S. "A Computational Study of the Hydrowy-Group Directivity in the Peroxyformic Acid Epoxidation of the Chiral Allylic Alcohol (Z)-3-Methyl-3-penten-2-ol: Control of Threo Diasteroselectivity through Allylic Strain and Hydrogen Bonding" *J. Org. Chem.,* **2000,** *65,* 6715-6728.

38. Cui, M.; Adam, W.; Shen, J. H.; Luo, X. M.; Tan, X. J.; Chen, K. X.; Ji, R. Y.; Jiang, H. L. "A Density-Functional Study of the Mechanism for theDiastereoselective Epoxidation of Chiral Allylic Alcohols by the TitaniumPeroxy Complexes" *J. Org. Chem.,* **2002**, *67,* 1427-1435.

39. Adam, W.; Alsters, P. L., Neumann, R.; SahaMoller, C. R. Sloboda-Rozner, D.; Zhang, R.; "A Highly Chemoselective, Diastereoselective, and Regioselective Epoxidation of Chiral Allylic Alcohols with Hydrogen Peroxide, Catalyzed by Sandwich-Type Polyoxometalates: Enhancement of Reactivity and Control of Selectivity by the Hydroxy Group through Metal-Alcoholate Bonding" *J. Org. Chem.,* **2003**, *68*, 1721-1728

40. Adam, W.; Alsters, P. L.; Neumann, R.; Saha-Moller, C. R.; Seebach, D.; Beck, A. K.; Zhang, R. "Chiral Hydroperoxides as Oxygen Source in the Catalytic Stereoselective Epoxidation of Allylic Alcohols by Sandwich-Type Polyoxometalates: Control of Enantioselectivity through a Metal-Coordinated Template" *J. Org. Chem.,* **2003**, *68*, 8222-8231.

41. Bach, R. D.; Armstrong, A.; Washington, I.; Houk, K. N. "Transition State Stereoelectronics in Alkene Epoxidations by Fluorinated Dioxiranes" *J. Am. Chem. Soc.,* **2003**, *122,* 6297-6298.

42. Sever, R. R.; Deubel, D. V.; Frenking, G.; Gisdakis, P.; Herrmann, W. A.; Rosch, N.; Sundermeyer, J. "Olefin Epoxidation with Inorganic Peroxides. Solutions to Four Long-Standing Controversies on the Mechanism of Oxygen Transfer*" Acc. Chem. Res.*, 2004, 37, 645-652.

43. Munakata, H.; Sankar, G.; Thomas, J. M.; Catlow, C. R. A.; Barker, C. M.; Gleeson, D.; Kaltsoyannis, N. "The Three-Dimensional Structure of the Titanium- Centered Active Site during Steady-State Catalytic Epoxidation of Alkenes" *J. Phys. Chem. B,* **2001**, *105,* 9028-9030.

44. Kudo, T.; Adam, W.; Alsters, P. L., Neumann, R.; SahaMoller, C. R. Sloboda- Rozner, D.; Zhang, R.; "A Highly Chemoselective, Diastereoselective, and Regioselective Epoxidation of Chiral Allylic Alcohols with Hydrogen Peroxide, Catalyzed by Sandwich-Type Polyoxometalates: Enhancement of Reactivity and Control of Selectivity by the Hydroxy Group through Metal-Alcoholate Bonding" *J. Org. Chem.,* **2003**, *68*, 1721-1728.

45. Iran, L. Quantum Chemistry, fifth ed. **(2000)**

46. Herhre, W. J.; Radom, L.; Schleyer, P. V. R.; Peple, J. A. Ab inintio Molecular Obital Theory. **(1986)**

APPENDIX

APPENDIX A

Determination of interplanar angle

The step of the transition structure for the oxygen transfer reaction indicated by the interplanar angle while is an angle between the vectors of planes V2O3O4 and O3C7C8 of TS3 (see Figure A1). The angle φ approach zero and ninety degree has actally called as the *spiro-* and *butterfly-* transition structure, respectively. The angle φ can be determined from the crossing of rectangular vector of the two planes V2O3O4 and O3C7C8.
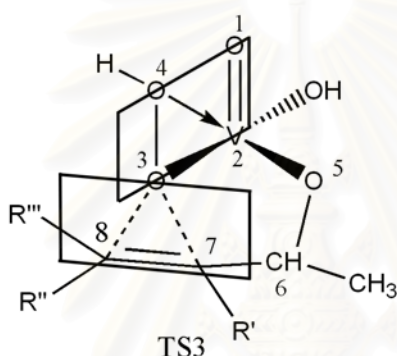

Figure A1. Atomic numbering of the transition structure 3 (TS3).

The procedure of determination of the angle φ of the transition structure 3 (TS3) as a sample is shown in figure A2.
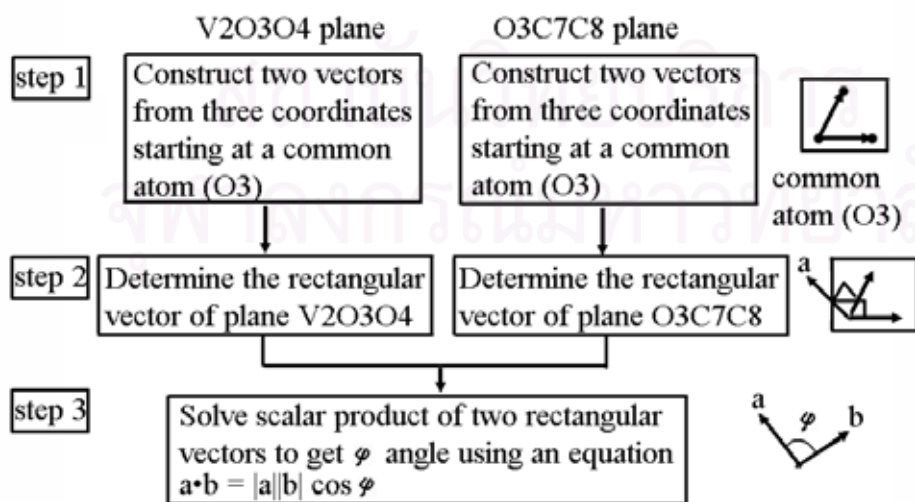

Figure A2. Schematic representation of methodology to solve φ angle

The example of determination of angle ϕ of ts3r1tb

Step 1:

    1.1. Select coordinate:

        V2 (1.03415, 0.333861, 0.683002)

        O3 (-0.45429, -0.80261, 1.055999)

        O4 (0.34631, -0.14801, 2.476493)

        C7 (-1.54635, -0.78217, -0.87659)

        C8 (-0.94567, -1.98029, -0.63927)

    1.2. Construct two vectors in plane V2O3O4:

        O3V2=(1.03415-(-0.45429),0.333861-(-0.80261),0.683002- 1.055999)

          =(1.488439, 1.136474, -0.37300)

        O3O4=(0.34631-(-0.45429),-0.14801-(-0.80261), 2.476493-1.055999)

          =(0.800599, 0.654605, 1.420494)

   Construct two vectors in plane O3C7C8 :

        O3C7=(-1.54635-(-0.45429),-0.78217-(-0.80261),-0.87659- 1.055999)

          =(-0.49138, -1.17768, -1.69527)

        O3C8=(-0.94567-(-0.45429),-1.98029-(-0.80261),-0.63927- 1.055999)

          =(-1.092059, 0.020442, -1.93259)

Step 2:

   Solve the rectangular vector of plane V2O3O4:

      a = **O3V2** $\wedge$ **O3O4** = (1.136474*0.800599 + (-0.37300) *0.654605,

      (-0.37300) * 0.800599+1.488439*1.420494,1.488439*0.654605+

      (-0.37300)* 0.800599)

     = (1.85852, -2.41294, 0.06448)

   Solve the rectangular vector of O3C7C8 plane

      b = **O3C7** $\wedge$ **O3C8**=(-1.17768 * (-1.092059) - (-1.69527)*0.020442,

              -1.69527 *(-1.092059)-(-0.49138)*(-1.93259),

              -0.49138 * 0.020442 - (-1.17768) * (-1.092059))

             =(2.310614, 0.901704, -1.29614)

<u>Step3:</u>

3.1. Calculate $|\mathbf{a}|$:

$$|\mathbf{a}| = (a_x^2 + a_y^2 + a_z^2)^{1/2} = (1.85852^2 + (-2.41294)^2 + 0.06448^2)^{1/2}$$
$$= 3.046397$$

3.2. Calculate $|\mathbf{b}|$:

$$|\mathbf{b}| = (b_x^2 + b_y^2 + b_z^2)^{1/2} = (2.310614^2 + 0.901704^2 + (-1.29614)^2)^{1/2}$$
$$= 2.798566$$

3.3. Solve scalar product of two rectangular vectors to get angle φ:

$$\mathbf{a} \cdot \mathbf{b} = |\mathbf{a}||\mathbf{b}| \cos \varphi = (a_x b_x + a_y b_y + a_z b_z)$$
$$= 1.85852 * 2.310614 + (-2.41294) * 0.901704 + 0.06448 * (-1.29614)$$
$$= 2.034992$$

$$\cos \varphi = \mathbf{a} \cdot \mathbf{b} / |\mathbf{a}||\mathbf{b}| = 2.034992 / (3.046397 * 2.034992)$$
$$= 0.23869$$

$$\varphi = arcos(\cos \varphi) = arcos (0.23869)$$
$$= 1.32978 \text{ radial or } 76.2 \text{ degree}$$

Therefore, the angle φ between planes V2O3O4 and O3C7C8 is 76.2 degree.

VITAE

NAME: Sirichai Lawanvisuth

DATE AND PLACE OF BIRTH: 3 June 1978 in Nakornphathom, Thailand.

ELEMENTARY SCHOOL:

1985-1990 Phathomthanbin Kamphangsan School, Nakornphathom.

SECONDARY SCHOOL:

1991-1993 Matthayomthanbin Kamphangsan School, Nakornphathom.

1994-1996 Sriboonyanoon School, Nonthaburi.

UNIVERSITY EDUCATION:

1997-2000 B. Sc. in Chemistry, Department of Chemistry, Faculty of Science,
Kasetsart University, Bangkok.

2002-2004 M. Sc. in Program of Petrochemistry and Polymer Science, Faculty of
Science, Chulalongkorn University, Bangkok.